Power Controllers for Wind Turbines Systems Based fn DFIG-Generators - A Review

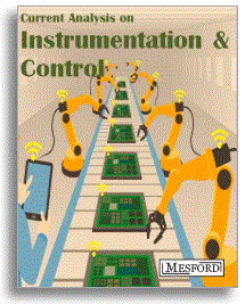

Badre Bossoufi[*‡], Mohammed Taoussi[**], Yasmine Ihedrane[**], Manale Bouderbala[*], Hala Alami Aroussi[*], Madiha El Ghamrasni[***]

** Laboratory of Electrical Engineering and Maintenance, Higher School of Technology, EST-Oujda, University of Mohammed I, Morocco.*
*** STIC Team, Faculty of Sciences Dhar El Mahraz, Sidi Mohamed Ben Abdellah University, Fez, Morocco.*

Abstract:

The objective of this article is to present the interest of the power regulation (active and reactive) of a wind system, for the improvement of the quality of produced energy to grid.

To this purpose, a variety of power control techniques, applied to the wind energy system based on the DFIG double feed asychronous generator are studied and developed. they consist of FOC controllers, a Backstepping controller, a Sliding Mode controller, and a Direct Torque Control (DTC) controller. The quality of the active and reactive power and the voltage of the wind system is significantly improved. a detailed study of the control techniques will be detailed and validate on the Matlab / Simulink environment with the simultaneous use of the "Pitch Control" and "MPPT" technique. Numerous results are given in order to illustrate the efficiency of the proposed solutions to achieve a high performance control of wind energy systems.

Publication History: Received: 11 August 2018 | Revised: 29 August 2018 |Accepted: 31 August 2018

Keywords:
DFIG-Generator, Backstepping Control, Adaptative control, DTC Control, Sliding Mode Control, Matlab/Simulink, Wind Turbine, MPPT.

1. INTRODUCTION

The climate change due to greenhouse emissions and the depletion risk of traditional fossil energy resources are two great challenges faced by the entire human society. The share of renewable energy sources (such as wind, sunlight, geothermal heat, hydropower, modern biomass) in energy supply has been growing rapidly during the recent years. At least 30 nations around the world already have renewable energy contributing more than 20% of their national energy supplies.

By reason of the fight against the green house effect and CO2 emissions into the atmosphere, renewables have experienced strong growth in recent years. Among these sources of energy are found " wind generators " that occupy a particular place [1, 2].

The wind power system using doubly fed induction generator composed by stator circuit connected directly to the network . A second rotor circuit is also connected to the network but via power converters [1, 4]. Since the rotor power transited is lower, the cost of the converters is reduced in comparison with a variable speed wind with a stator circuit connected to the network by power converters.This is the main reason why we find this generator for the production of high power. A second reason is the ability to adjust the voltage at the connection point of this generator [3-6].

Nowadays, Doubly-Fed Induction Generator (DFIG) has been widely installed in wind turbine farms for the production of electric power due to high efficiency, energy quality and the possibility of controlling the power supplied to the grid [1, 27, 2]. The disadvantage of the wind turbine based on DFIG is that it is very sensitive to load disturbances, the variation of the speed's rotation of the turbine and the variation of the internal and external parameters of the system. Similarly, the system is multi-variable, dynamic, very coupled and non-linear which makes the control of it very difficult [3]. However, the development and multiplication of wind turbines have led researchers to improve the efficiency of electromechanical conversion and the quality of the energy supplied by different controls [4]. The main idea of this approach is to analyze the stability of the nonlinear system without solving the differential equations of this system. It is a very powerful tool to test and find sufficient conditions for the stability of different dynamic systems. The study presented in this paper aims to optimize the

*Address correspondence to this author at the Badre BOSSOUFI, Université Mohammed I, Ecole Supérieure de Technologie, Complexe Universitaire Al Qods 60000-Oujda, Maroc Tel: +212 663 48 40 13; E-mail: badre_isai@hotmail.com

Mesford Publisher Inc
Office Address: Suite 2205, 350 Webb Drive, Mississauga, ON L5B3W4, Canada; T: +1 (647) 7109849 |E: caic@mesford.ca, contact@mesford.ca, https://mesford.ca/journals/caic/

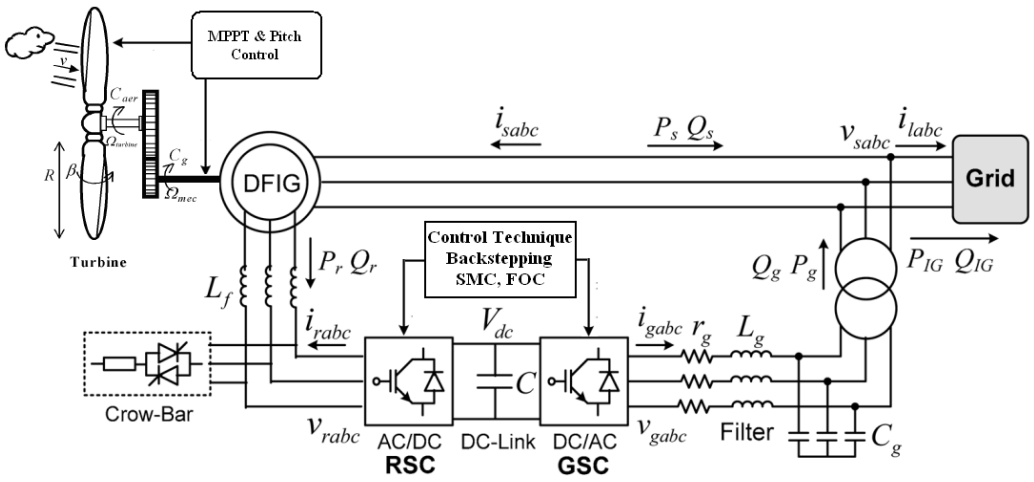

Fig. (1). Architecture of the Control.

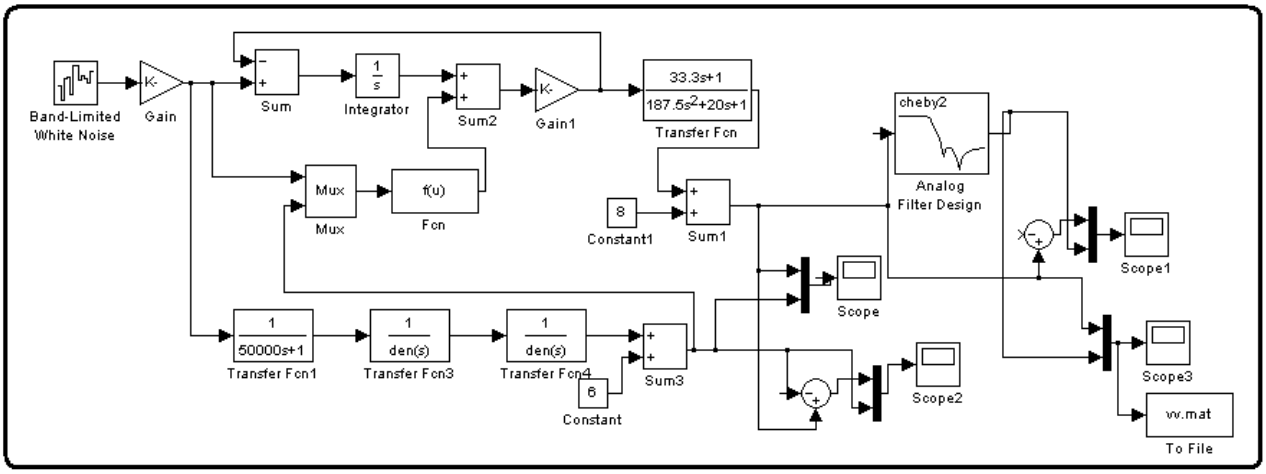

Fig..(2). Model developed on Simulink for the generation of the reference wind speed.

energy performance of a wind turbine in order to maximize the wind energy captured while reducing structural problems cited previously and improving control performance by reducing time of calculation. This optimization is capable to minimize the costs of electricity production.

In this article, we begin with a wind turbine modeling, then a study of the operating point tracking technique and maximum power will be presented. Subsequently, we present a DFIG model in the "dq" benchmark, and the general principle of controlling both power converters that is based on the control strategy.

In this work, we develop three control strategies namely Filtered Oriented Control (FOC), Backstepping Control and Sliding Control Mode. A study of the control technique is presented and developed by Matlab / Simulink. Finally, the results are presented and analyzed. The fig. (**1**) shows the detailed structure of the wind energy conversion system.

2. WIND TURBINE MODELLING

2.1. Wind Speed Model

It is very difficult, if not almost impossible, to predict the change in wind speed at a given site. Over a relatively long period, the model of the wind speed is represented by 2 components: a slow or seasonal component; - And a component of turbulence. This modeling methodology has been widely developed in [3-5], we will only repeat here the final result. Two solutions emerged: one using a non-rational transfer function filter in the modeling process of the turbulence component, and the other using an adaptation of the filter with a rational transfer function. Modeling with non-rational filter is not suitable for real-time simulation, because of the cost in computing time of the algorithm; this is why it is the solution with rational filter that has been chosen for this thesis. Below, we present a wind speed profile using the second modeling method:

2.2. Modelling of the Wind Turbine Power

The wind turbine power production depends on interaction between the mechanical power extracted from the wind and the incident wind power (PWind) [9, 22]. The expression for the mechanical power captured by the wind turbine and transmitted to the rotor (PRotor), is expressed by:

$$\begin{cases} P_{Rotor} = P_{Wind}.C_p(\lambda,\beta) \\ P_{Wind} = \frac{1}{2}\rho.S.v^3 \end{cases} \Rightarrow P_{Rotor} = \frac{1}{2}\rho.S.C_p(\lambda,\beta).v^3 \qquad (1)$$

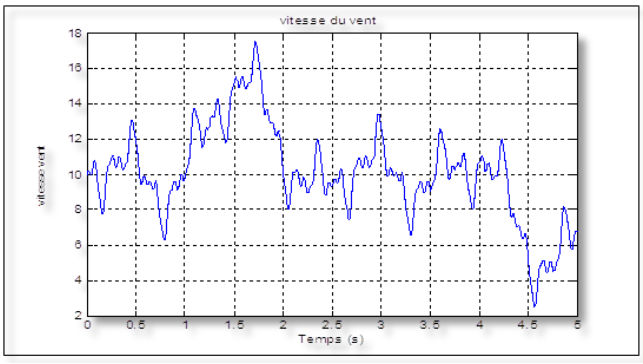

Fig. (3). wind speed reference.

With Cp (λ,β) is the power coefficient, v is the wind speed (m/s), ϱ is the air density and S is the area swept by blades (m2)

Betz proved that the maximum extractable power for a given wind speed by ideal turbine and conditions is Cpmax(λ,β)=0.593, this limit is known as the Betz limit. For the DFIG, the power coefficient (Cp(λ , β)) is possible to model with a single equation that depends on the tip speed ratio (λ) and the pitch angle (β) of the blades. This can be written as:

$$C_p(\lambda,\beta) = c_1.\left(c_2.\frac{1}{A} - c_3.\beta - c_4\right).e^{-c_5\frac{1}{A}} + c_6.\lambda \qquad (2)$$

With: $\begin{cases} c_1 = 0.5872 \\ c_2 = 116 \\ c_3 = 0.4 \\ c_4 = 5 \\ c_5 = 21 \\ c_6 = 0.0085 \end{cases}$ And $\begin{cases} \frac{1}{A} = \frac{1}{\lambda + 0.08.\beta} - \frac{0.035}{1+\beta^3} \\ \lambda = \frac{\Omega_t.R}{v} \end{cases}$

Refer to Fig.(**2**), the wind system will provide optimal electrical power characterized by the $C_p^{max}(12,0) = 0.5506$.

- Wind Turbine.

The wind turbine is characterized by the curves of the coefficient power, which corresponds to the aerodynamic torque (TRotor), shown in Eq (3).

$$T_{Rotor} = \frac{P_{Rotor}}{\Omega_t} = \frac{1}{2}\rho.S.C_p(\lambda,\beta).v^3.\frac{1}{\Omega_t} \qquad (3)$$

- Gearbox.

To adapt the speed of the turbine, to that of the generator, is necessary to connect the wind turbine and the DFIG to the Gearbox. It is modelled by the following two equations:

$$\begin{cases} \Omega = G.\Omega_t \\ T_{Rotor} = G.T_m \end{cases} \qquad (4)$$

Shaft

The evolution of the generator speed (Ω) depends on the fundamental equation of the dynamics that characterizes the mechanical behaviour of the turbine and generator from the total mechanical torque applied to the rotor. It is given by the following formula:

$$J\frac{d\Omega}{dt} = T_m - T_{em} - f.\Omega \qquad (5)$$

3. MODELLING OF THE DFIG

For a better modelling of a doubly-fed induction generator (DFIG), it is necessary to use a specific, generic model and simple. In the stationary "abc" reference frame, the relationships between the voltages, currents, and flux linkages of each phase of this machine, are time variant [11]. The time variant quantities can be made time invariant by transforming them into an appropriate rotating reference frame "dq". Using park transforms, can be written from equations below [29].

3.1. Electrical Equations of Stator

The equations of the stator in the reference (d,q), are expressed by:

- Stator voltage:

$$\begin{cases} V_{sd} = R_s.I_{sd} + \frac{d\phi_{sd}}{dt} - \omega_s.\phi_{sq} \\ V_{sq} = R_s.I_{sq} + \frac{d\phi_{sq}}{dt} + \omega_s.\phi_{sd} \end{cases} \qquad (6)$$

- Stator current:

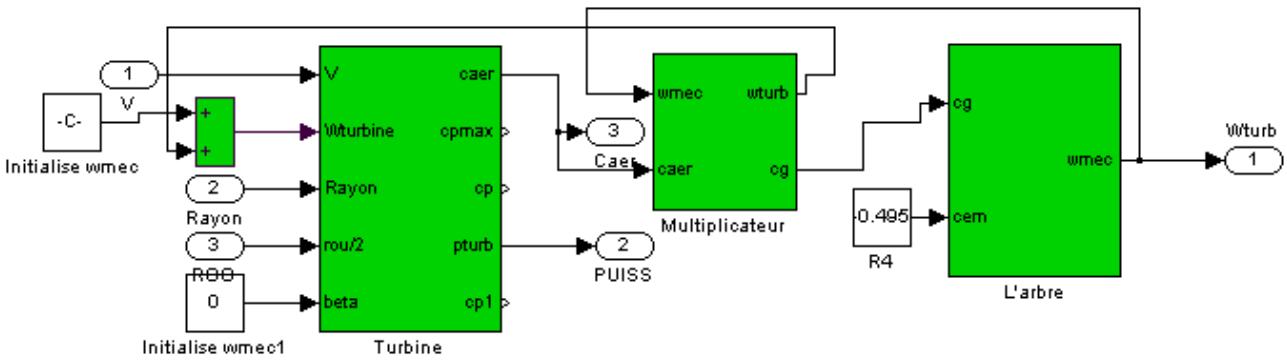

Fig. (4). Wind-turbine model.

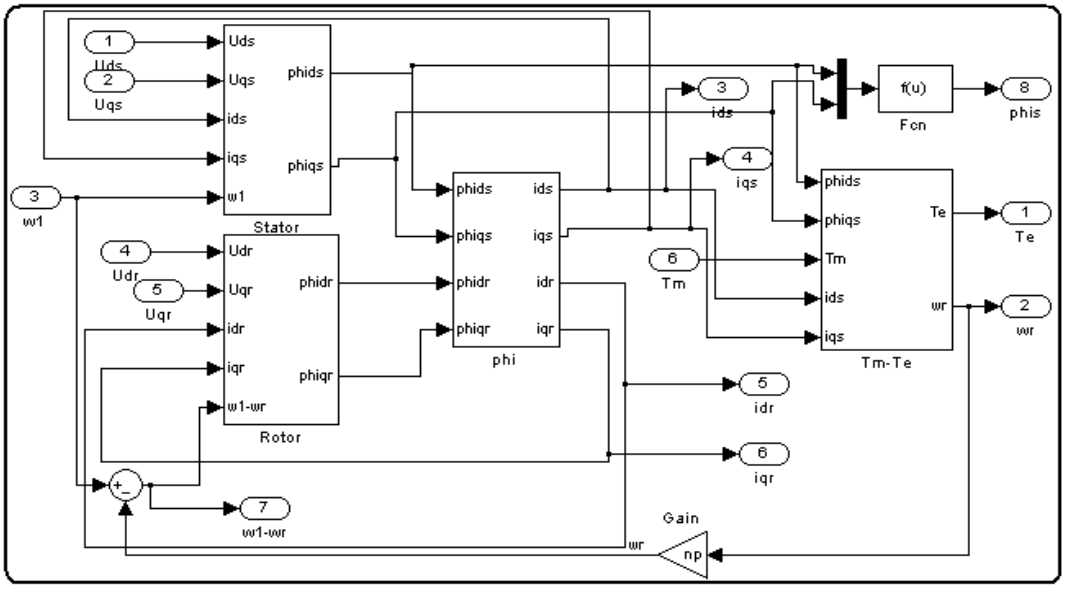

Fig. (5). DFIG-Generator Model.

$$\begin{cases} I_{sd} = \dfrac{1}{\sigma.L_s}.\phi_{sd} - \dfrac{M}{\sigma.L_r}.\phi_{rd} \\ I_{sq} = \dfrac{1}{\sigma.L_s}.\phi_{sq} - \dfrac{M}{\sigma.L_s.L_r}.\phi_{rq} \end{cases} \quad (7)$$

- Stator flux:

$$\begin{cases} \phi_{sd} = L_s.I_{sd} + M.I_{rd} \\ \phi_{sq} = L_s.I_{sq} + M.I_{rq} \end{cases} \quad (8)$$

- Stator power:

$$\begin{cases} P_s = \dfrac{3}{2}\left(V_{sd}.I_{sd} + V_{sq}.I_{sq}\right) \\ Q_s = \dfrac{3}{2}\left(V_{sq}.I_{sd} - V_{sd}.I_{sq}\right) \end{cases} \quad (9)$$

3.2. Electrical Equations of Rotor

The equations of the rotor in the reference (d, q), are expressed by:

- Rotor voltage:

$$\begin{cases} V_{rd} = R_r.I_{rd} + \dfrac{d\phi_{rd}}{dt} - \omega_r.\phi_{rq} \\ V_{rq} = R_r.I_{rq} + \dfrac{d\phi_{rq}}{dt} + \omega_r.\phi_{rd} \end{cases} \quad (10)$$

- Rotor courant :

$$\begin{cases} I_{rd} = \dfrac{1}{\sigma.L_r}.\phi_{rd} - \dfrac{M}{\sigma.L_r.L_s}.\phi_{sd} \\ I_{rq} = \dfrac{1}{\sigma.L_r}.\phi_{rq} - \dfrac{M}{\sigma.L_r.L_s}.\phi_{sq} \end{cases} \quad (11)$$

- Rotor flux:

$$\begin{cases} \phi_{rd} = L_r.I_{rd} + M.I_{sd} \\ \phi_{rq} = L_r.I_{rq} + M.I_{sq} \end{cases} \quad (12)$$

- Rotor power:

$$\begin{cases} P_r = \dfrac{3}{2}\left(V_{rd}.I_{rd} + V_{rq}.I_{rq}\right) \\ Q_r = \dfrac{3}{2}\left(V_{rq}.I_{rd} - V_{rd}.I_{rq}\right) \end{cases} \quad (13)$$

3.3. Mechanical Equations

The electromechanical torque in the rotor can be determined by the following relationship:

$$\begin{cases} T_{em} = T_m + J.\dfrac{d\Omega}{dt} + f.\Omega \\ T_{em} = p(I_{sd}.\phi_{sq} - I_{sq}.\phi_{sd}) \end{cases} \quad (14)$$

4. PITCH CONTROL AND MPPT CONTROLLER

4.1. Pitch Control Techchnique

The manufacturers use two control systems to limit the power extracted by the generator to its nominal value:

- An aerodynamic stall system consisting of designing the blades with a shape to increase the lift losses from a certain wind speed.
- A system of orientation of the blades making it possible to modify the angle of setting of the blades according to the speed of the wind with a view to maintaining the power extracted by the generator at its nominal value.

The aerodynamic stall system is generally used for low speed fixed speed wind turbines. Builders justify this choice by the fact that this system is more economical.

The blade orientation system is mainly used by high power devices with variable speed. In the latter case, the blade is rotated using a control device known as the "pitch control".

Comparing the two systems, the pitch control technique has many advantages:

- It allows a higher production of energy with high wind speeds.
- It allows active power control for wide speed variations.
- It facilitates braking.
- It reduces the mechanical forces during operation under nominal power and under high speeds.

The power extracted by the turbine is therefore represented by the figure below:

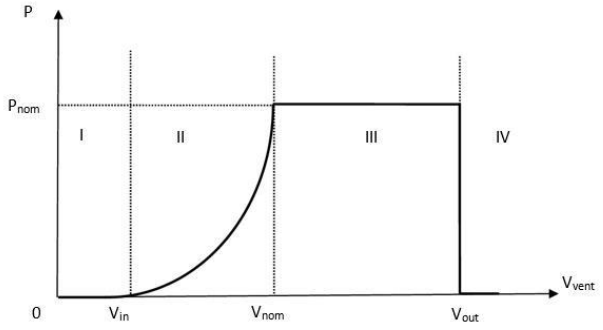

Fig. (6). Power extracted from the wind according to the wind speed.

- ✓ Zone I is the starting zone of the turbine. Indeed, below the minimum wind speed necessary for its start (Vin), the turbine does not work (P = 0)
- ✓ In zone II, the power of the turbine increases according to the speed of the wind until to reach its nominal value
- ✓ In zone III, whatever the wind speed between Vnom and Vout, the power must remain at its nominal value.
- ✓ In Zone IV, beyond Vout, a safety device causes the shutdown of the turbine to preserve the integrity of the system against the force of the wind.

The control of the wedging angle is therefore in zone III in order to limit by means of the orientation of the blades of the turbine, the power extracted has a value called nominal value.

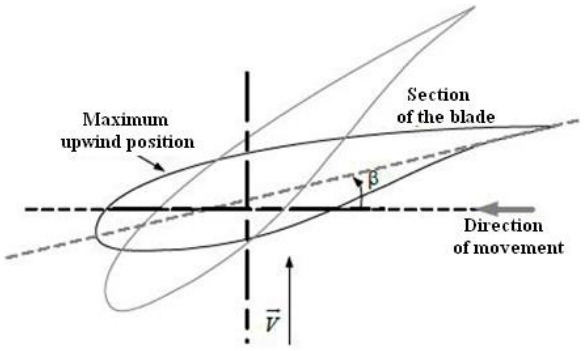

Fig. (7). Variation of the β angle of a blade.

Below, we present the influence of the variation of the angle of setting on the value of the coefficient of power which represents the energy efficiency of the turbine:

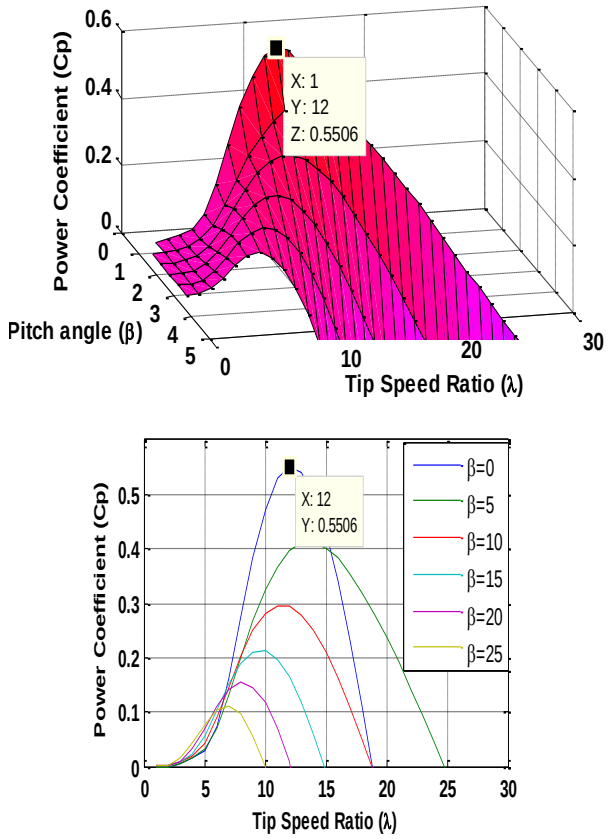

Fig. (8). Influence of the β angle on the power coefficient.

It can be seen that as the wedging angle increases, the efficiency of the turbine decreases. The control of the β wedge angle for the orientation of the blades of the turbine can be achieved at a single control loop or two controls loops:

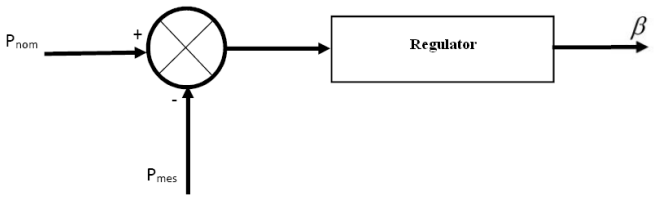

Fig. (9). Control of the β angle has a regulation loop.

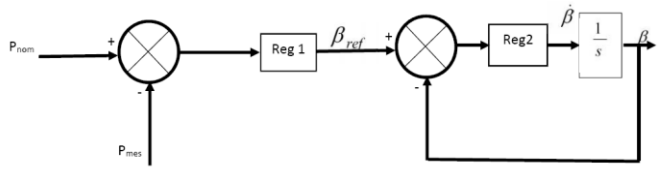

Fig. (10). Control of the β angle has two regulation loops.

When the control is performed at a single control loop, this is the control of the nominal power. The output of the regulator of the nominal power then corresponds to the reference value of the β angle, and is transmitted to the system of orientation of the blades by an open-loop control.

When the control is carried out with two control loops, the first corresponds to the regulation of the nominal power, and the second to the regulation of the calibration angle.

The second control mode is more complex to implement in terms of the synthesis of regulators, and more, it is more expensive since it requires the use of two regulators for its control.

4.2. MPPT Strategy

We have seen above that the extraction of wind power depended on the value of the power coefficient. According to the characteristics power - speed of rotation of a given turbine represents in the figure below:

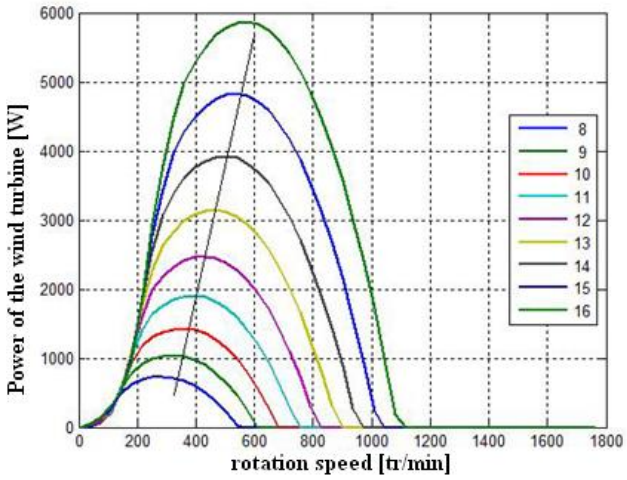

Fig. (11). MPPT-Power of Wind Turbine.

It can be seen that for each value of wind speed V, the characteristic power - rotational speed passes through a maximum corresponding to a maximum power reached for an optimal rotational speed. However, the maximum power is obtained for a maximum power coefficient:

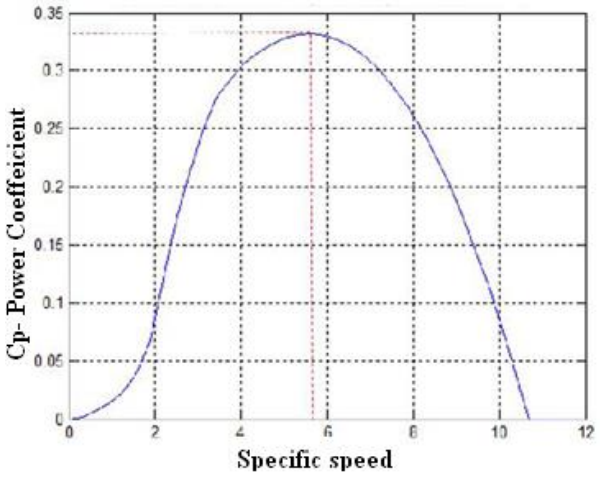

Fig. (12). MPPT- Coefficient of Power Cp.

This maximum value of the power coefficient corresponds to an optimal specific speed λopt. This specific speed is obtained for an optimal speed of rotation:

$$\Omega_{opt} = \frac{\lambda_{opt}.V}{R}$$

It is this optimal value of the speed of rotation which is sent as a reference for the speed control of the electric machines. The speed control of the electrical machines can be achieved either in scalar control or in vector control (also called directed flow). The scalar command is used for the steady-state control while the vector control is used in transient mode. As part of this thesis, we opted for vector control, since the models used are developed under transient conditions, the control is more precise and faster, and moreover it allows controlling the magnitudes in amplitude and phase.

The control of the static converter on the machine side makes it possible to control the torque of the generator in order to obtain the desired speed of rotation for the extraction of the maximum power. This consists in controlling the electric machine by a general cascade structure with nested loops.

Torque and flux will therefore be controlled by very fast internal current loops. These commands are carried out in a rotating repository (vector control with flux oriented). The torque setpoint is obtained from a slower external speed control loop. As for the speed reference, it is calculated from a MPPT strategy as presented above.

5. FIELD ORIENTED POWER CONTROL

5.1. Principle of Control

The principle of control by stator field direction is to orient the stator field along the axis 'd' [20], that is to say : Φsd = Φs and Φsq = 0.

For medium and large wind turbines, the stator resistors are negligible, and also the flow becomes constant. For this, the flux have as an expression:

$$\begin{cases} \phi_{sq} = 0 = L_s.I_{sq} + M.I_{rq} \\ \phi_{sd} = L_s.I_{sd} + M.I_{rd} \end{cases} \quad (15)$$

From equation (6) and (15), we obtain:

$$\begin{cases} I_{sq} = -\frac{M}{L_s} I_{rq} \\ I_{sd} = \frac{1}{L_s}(\varphi_s - M.I_{rd}) \end{cases} \quad (16)$$

The expression of electromagnetic torque [13]:

$$C_{em} = p.\varphi_s.I_{sq} = -p\frac{M}{L_s}\varphi_s I_{rq} \quad (17)$$

Based on the assumptions:

$$\begin{cases} V_{sd} = 0 \\ V_{sd} = V_s = \omega_s.\varphi_s \end{cases} \Rightarrow \varphi_s = \frac{V_s}{\omega_s} \quad (18)$$

The stator active and reactive powers are written according to following expressions [13]:

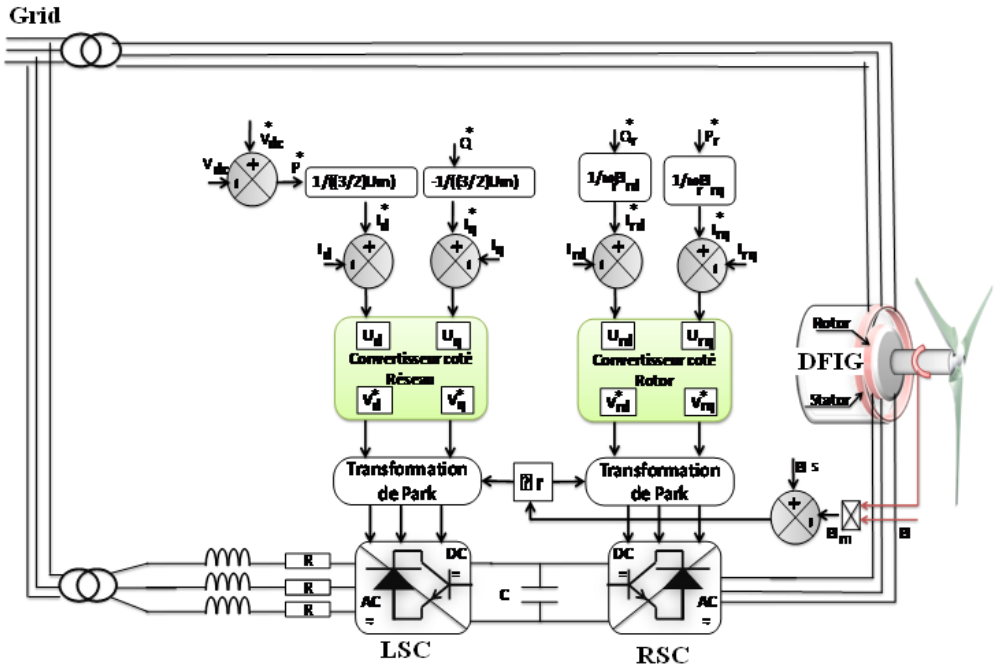

Fig. (13). FOC Control Modelling.

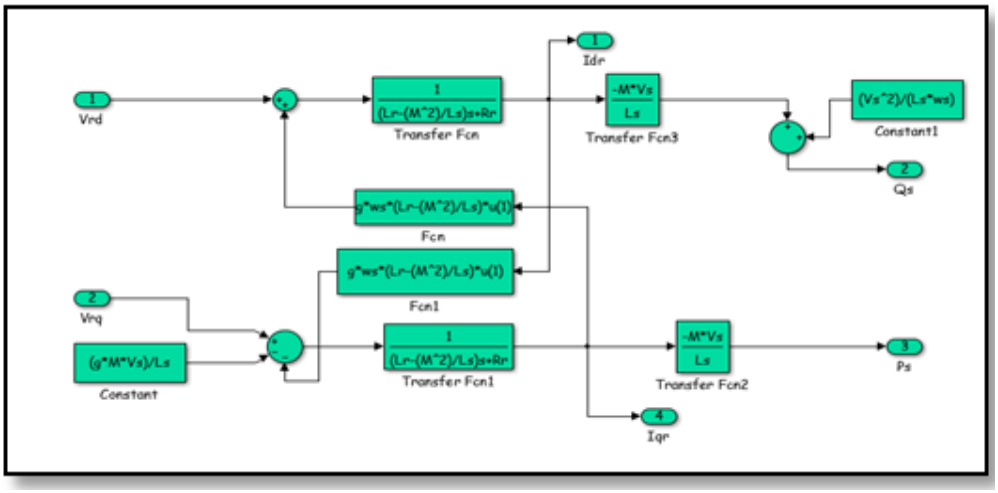

Fig. (14). Block diagram of the DFIG.

$$\begin{cases} P_s = V_{sd}.I_{sd} + V_{sq}.I_{sq} \\ Q_s = V_{sq}.I_{sd} - V_{sd}.I_{sq} \end{cases} \quad (19)$$

By replacing the equation (19) by (15), (16) and (18), we get following expression of power [13]:

$$\begin{cases} P_s = V_s.I_{sq} = -V_s.\dfrac{M}{L_s}.I_{rq} \\ Q_s = V_s.I_{sd} = \dfrac{V_s^2}{\omega_s L_s} - V_s.\dfrac{M}{L_s}.I_{rd} \end{cases} \quad (20)$$

The expression of the rotor field becomes:

$$\begin{cases} \varphi_{rd} = (L_r - \dfrac{M^2}{L_s}).I_{rd} + M\dfrac{V_s}{\omega_s L_s} \\ \varphi_{rq} = (L_r - \dfrac{M^2}{L_s}).I_{rq} \end{cases} \quad (21)$$

From these equations we can deduce the relation between the rotor voltages (d, q) and the rotor currents (d, q):

$$\begin{cases} V_{rd} = \left(R_r + S.(L_r - \dfrac{M^2}{L_s})\right).I_{rd} - \omega_s.g.(L_r - \dfrac{M^2}{L_s}).I_{rq} \\ V_{rq} = \left(R_r + S.(L_r - \dfrac{M^2}{L_s})\right).I_{rq} - \omega_s.g.(L_r - \dfrac{M^2}{L_s}).I_{rd} \\ +g.\dfrac{M}{L_s}.V_s \end{cases} \quad (22)$$

The following figure shows the block on Simulink that models the equations defined previously:

The following figure shows the equation of the machine, using first-order transfer functions for voltages. The vector control will be easily implemented later, considering the negligible value of the slip g and the influence of the coupling and weak.

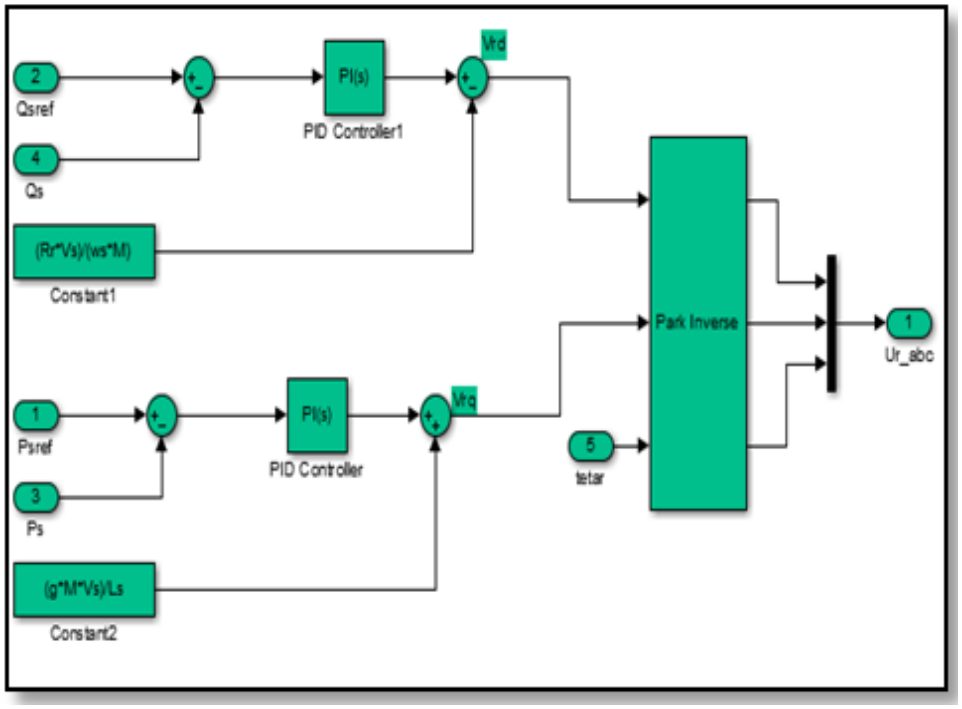

Fig. (15). Direct vector control.

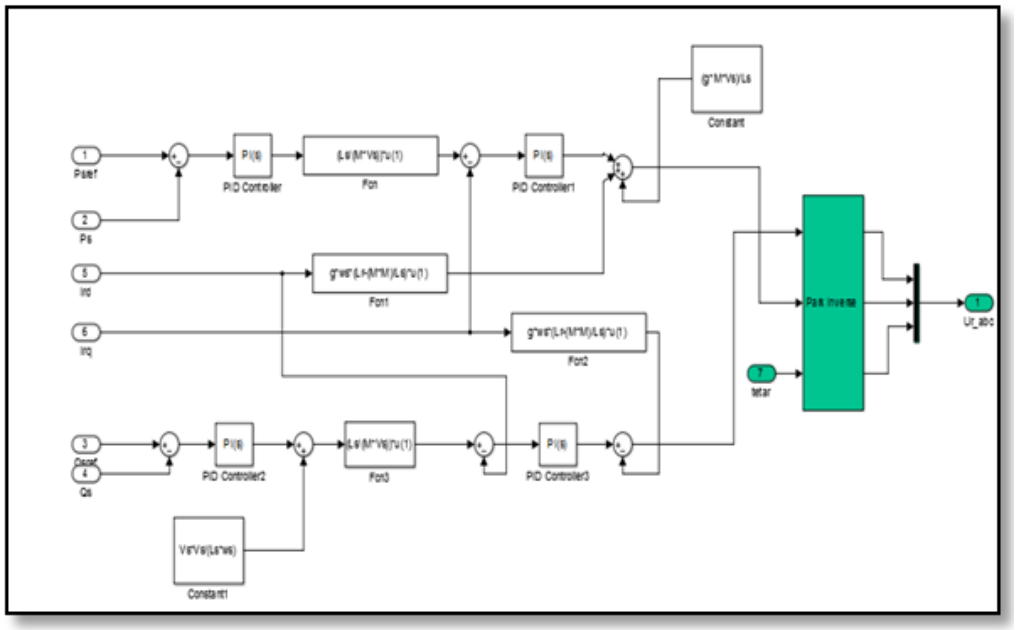

Fig. (16). Indirect Field Oriented Control.

5.2. FOC Control Technique

In this work, we use two types of vector control. The first is a direct control, which is based on the use of a PI regulator in each axis to independently control the active and reactive power of the system. The regulators in this case directly control the rotor voltage of the DFIG.

The second method is to consider the coupling terms and compensate them performing a system with two loops to control the powers and rotor currents. This method which is called Indirect Method [4] is generated directly from equations (19) and (21).

5.3. Simulations Results

In this part, we present the simulation results of the proposed model for direct and indirect control (FOC).

The simulation results are summarized in Fig. (**16** and **17**):

According to (fig. **19**), we see that the power steps are followed by the generator both for the active and reactive powers. We also see that the stator active power Ps depends on the quadrature rotor current Iqr and the stator reactive power Qs depends on the direct rotor current Idr and there the effect of coupling is also observed between the two control axes d and

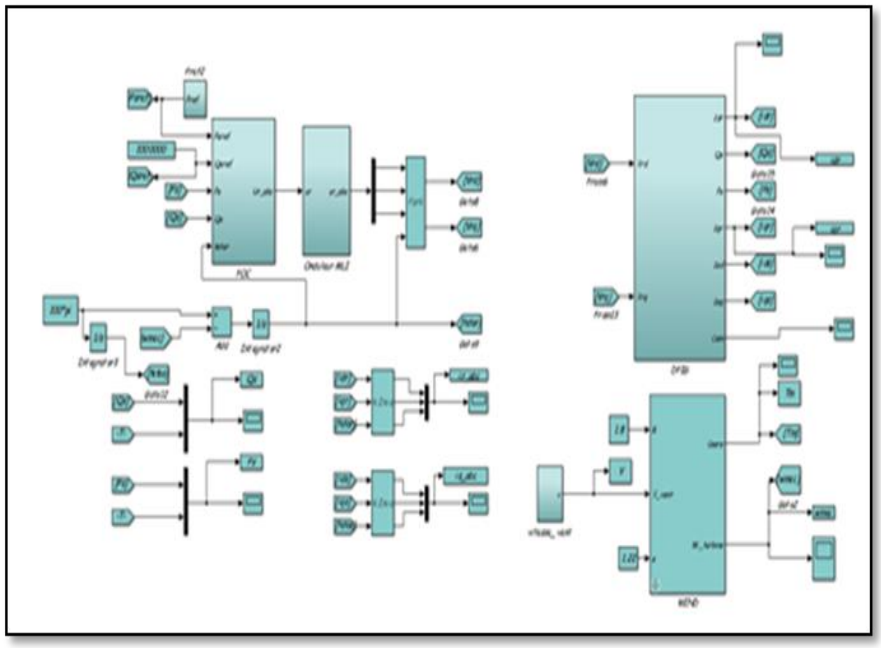

Fig. (17). Wind System and direct field oriented control with MATLAB /SIMULINK.

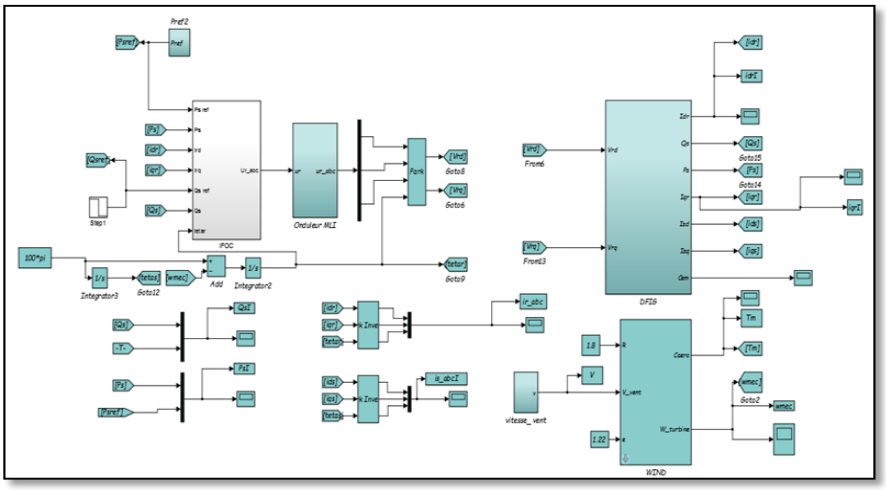

Fig. (18). Wind System and indirect field oriented control with MATLAB /SIMULINK.

q. The active and reactive powers of the stator side are adjustable depending on network requirements. In our case it is negative, which means that the network is a receiver of the energy supplied by the DFIG.

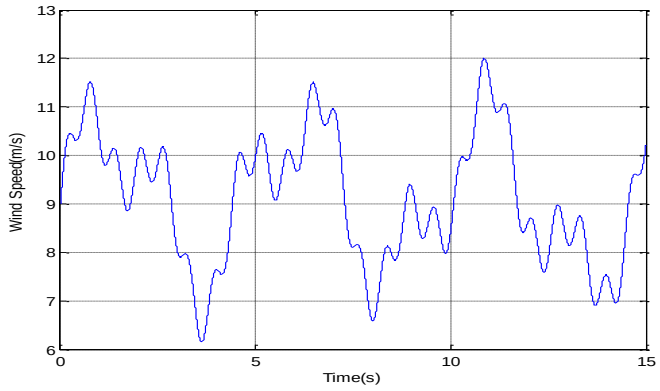

Fig. (19a). Wind profile.

The (Fig. **20**) shows that our system has satisfactory dynamics which react rapidly, without overtaking and the static error is almost zero for both the active or reactive powers. The coupling between the two powers is very low and barely perceptible.

6. BACKSTEPPING POWER CONTROLLER

6.1. Principe of Control

The basic principle of the adaptive Backstepping control is to move from nonlinear system to a linear system, without even solving differential equations of the system. This control is based on the second method of Lyapunov technique, that makes loop systems equivalent to command subsystems stable, this technique is a very powerful tool to test the stability of the different dynamic systems [12, 28]. The adaptive Backstepping control depends only on the study of different variations of the system, by finding the equivalent function along the trajectory of the system, using estimation and observation, to ensure the

convergence of the system to its equilibrium state which gives it the qualities of robustness and global asymptotic stability [13, 26]. For details, we take such an example:

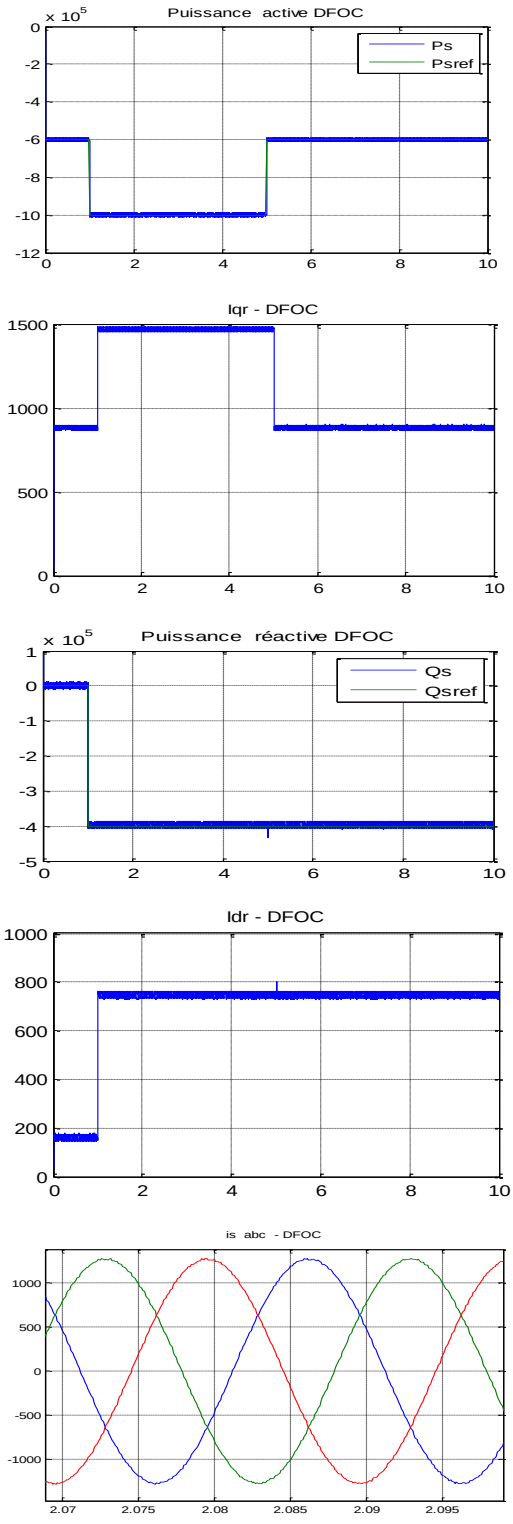

Fig. (19b). Direct Field Oriented Control.

$$\begin{cases} \dot{x}_1 = f(x_1) + x_2 \\ \dot{x}_2 = u \end{cases} \quad (23)$$

With, the system is characterized by:

$$\begin{cases} \begin{bmatrix} x_1 & x_2 \end{bmatrix}^T : \text{State vector.} \\ u \quad : \text{Control vector.} \\ x_1 = x_2 = 0 : \text{Equilibrium point of the system.} \end{cases}$$

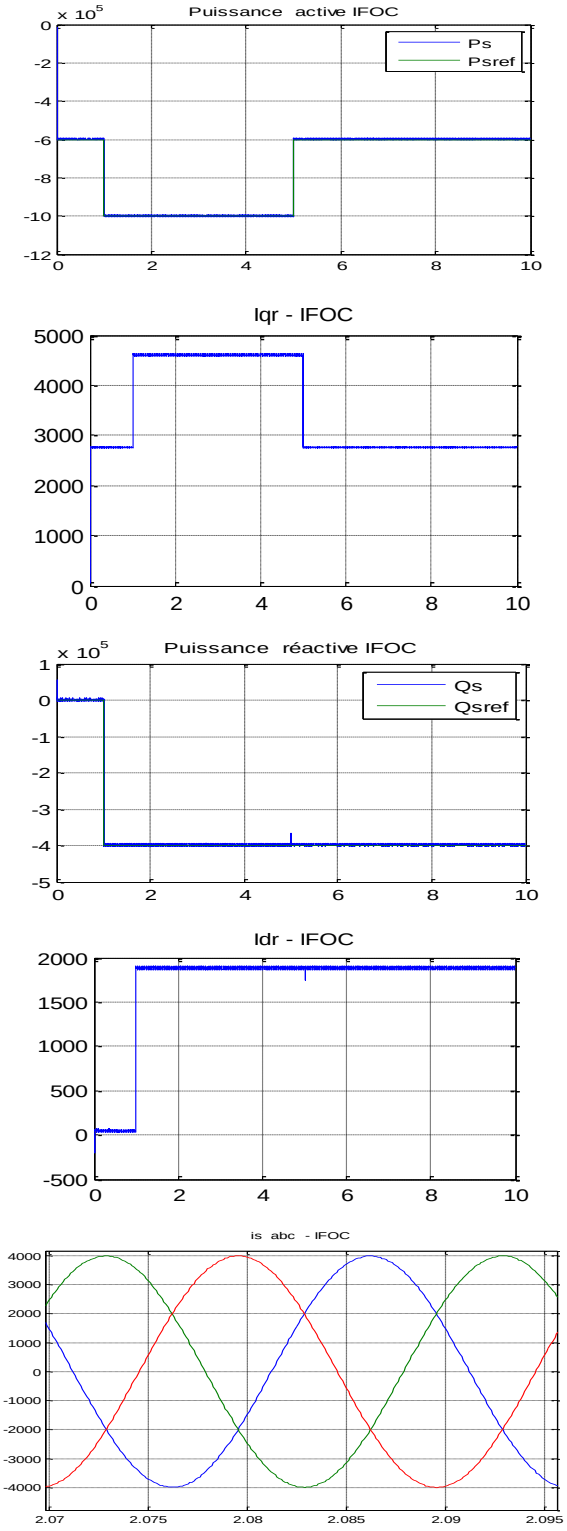

Fig. (20). Indirect Field Oriented Control Results.

The application of the Lyapunov function for this system, which contains the equation (16), is done in two steps.

- Step 1:

In this step, for stability of the system, we seek to constitute the first Lyapunov function V1 and to guarantee the negativity of derive the Lyapunov function V1; therefore the error must converge to 0. The first Lyapunov function V1 as a quadratic form:

$$V_1 = \frac{1}{2}(x_{1d} - x_1)^2 = \frac{1}{2}e_1^2 \tag{24}$$

e_1 : tracking error.

x_{1d} : output of a desired trajectory.

Which the derivative of the Lyapunov function is:

$$\dot{V}_1 = e_1\dot{e}_1 = e_1(\dot{x}_{1d} - \dot{x}_1) = e_1(\dot{x}_{1d} - f(x_1) - x_2) \tag{25}$$

In order to guarantee the negativity of the derivative of the Lyapunov function V1, we defined for this a positive constant conception K1 such:

$$\dot{V}_1 = -K_1e_1^2 + e_1(K_1e_1 + \dot{x}_{1d} - f(x_1) - x_2) \tag{26}$$

For the stability of the system, we defined the virtual command x2k as follows:

$$x_{2k} = K_1e_1 + \dot{x}_{1d} - f(x_1) \tag{27}$$

So the derivative of the Lyapunov function becomes:

$$\dot{V}_1 = -K_1e_1^2 + e_1(x_{2k} - x_2) \tag{28}$$

We define a new variable to the previous virtual control. It is a new regulation error e2 defined by the following equation:

$$e_2 = x_{2k} - x_2 \tag{29}$$

To take account for this error e2, the Lyapunov function V1 is increased by another term V2, in the second step.

- Step 2:

The function V2 is a new Lyapunov function of the system represented by the equation (16).

$$V_2 = \frac{1}{2}e_1^2 + \frac{1}{2}e_2^2 \tag{30}$$

With: $\begin{cases} e_1 = x_{1d} - x_1 \\ e_2 = x_{2k} - x_2 \end{cases}$

Its derivative allows the convergence of the error to zero, such as:

$$\begin{aligned} \dot{V}_2 &= e_1\dot{e}_1 + e_2\dot{e}_2 = e_1(e_2 - K_1e_1) + e_2(K_1\dot{e}_1 + \ddot{x}_{1d} - \dot{f}(x_1) - u) \\ &= e_1(e_2 - K_1e_1) + e_2(K_1(e_2 - K_1e_1) + \ddot{x}_{1d} - \dot{f}(x_1) - u) \\ &= -K_1e_1^2 + e_2(e_1 + K_1e_2 - K_1^2e_1 + \ddot{x}_{1d} - \dot{f}(x_1) - u) \end{aligned} \tag{31}$$

With: $\begin{cases} e_2 = K_1e_1 + \dot{x}_{1d} - f(x_1) - x_2 = K_1e_1 + \dot{e}\dot{e}_1 \\ \dot{e}_2 = \dot{x}_{2k} - \dot{x}_2 = K_1\dot{e}_1 + \ddot{x}_{1d} - \dot{f}(x_1) - \dot{x}_2 \\ u = \dot{x}_2 \end{cases}$

$$\Rightarrow \dot{e}_2 = K_1\dot{e}_1 + \ddot{x}_{1d} - \dot{f}(x_1) - u \tag{32}$$

With, u: is the control law.

To ensure the negativity of the Lyapunov function (23), it is necessary that the expression in brackets (24) must be equal to -K2e2, (K2> 0 is the constant design). In this case, the control's law is described as follows:

$$\begin{aligned} u &= K_2e_2 + e_1 + K_1e_2 - K_1^2e_1 + \ddot{x}_{1d} - \dot{f}(x_1) \\ &= e_2(K_1 + K_2) + e_1(1 - K_1^2) + \ddot{x}_{1d} - \dot{f}(x_1) \end{aligned} \tag{33}$$

This ensures that the negative of the derivative of the Lyapunov function is:

$$\dot{V}_2 = -K_1e_1^2 - K_2e_2^2 \le 0 \tag{34}$$

The overall advantage of the Backstepping control is its flexibility with a good choice of K1et K2 gains. Then it gives an asymptotic stability to the original and the outputs of the system follow the reference value. The main idea of the adaptive Backstepping control is demonstrated by its application to the doubly-fed induction generator (DFIG).

6.2. Application of Adaptive Backstepping Controls for DFIG-Generator

This part consists on establishing a control's law of the machine DFIG via a Lyapunov function selected. It has the advantage of being robust with the parametric variations of the machine and a good continuation of the references [14]. The association of adaptive Backstepping control and orientation of rotor flux confirmed the good qualities of robustness and consolidates the overall stability of the system [31]. The purpose of adaptive Backstepping control is to regulate the active and reactive power of DFIG to their reference values [15, 20, 23, 25]. We suppose in this search that machine's parameters are constants and known. The general structure of the control's laws with the references is detailed in the Fig. (**19**):

6.3. Application of the Backstepping Control to the Rotor-Side Converter(RSC).

The main objective of the control to the rotor side converter is to operate the wind turbine almost exactly at the nominal power. For this, it is necessary to control the active and reactive powers of stator by calculating and controlling the rotor's voltages. According to the electrical Eq. (10) of the DFIG, we can calculate the following expressions of the instantaneous variations of the reactive and active powers of the stator:

$$\begin{cases} \dfrac{dP_s}{dt} = \dfrac{3}{2}\left[\dfrac{dV_{sd}}{dt}.I_{sd} + \dfrac{dI_{sd}}{dt}V_{sd} + \dfrac{dV_{sq}}{dt}.I_{sq} + \dfrac{dI_{sq}}{dt}V_{sq}\right] \\ \dfrac{dQ_s}{dt} = \dfrac{3}{2}\left[\dfrac{dV_{sq}}{dt}.I_{sd} + \dfrac{dI_{sd}}{dt}V_{sq} - \dfrac{dV_{sd}}{dt}.I_{sq} - \dfrac{dI_{sq}}{dt}V_{sd}\right] \end{cases} \tag{35}$$

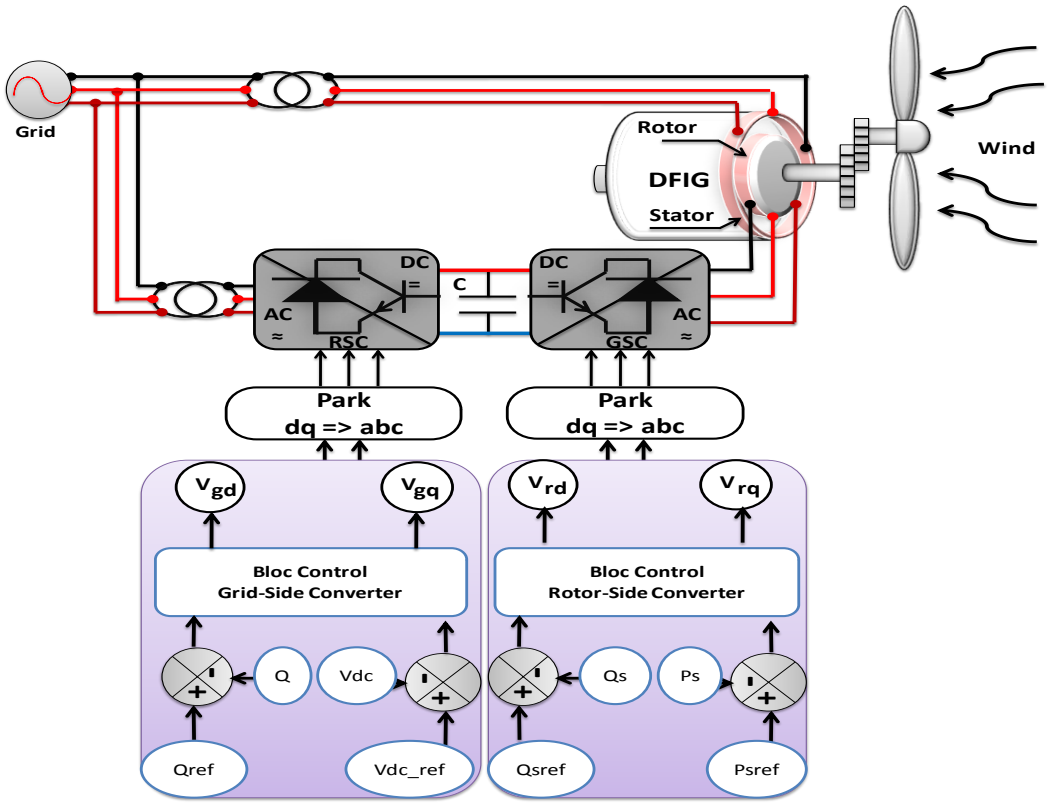

Fig. (21). General structure of the control for the wind turbine system.

The instantaneous stator current variations can be expressed by substituting, the equations (9) and (13) into (7) and (11), we obtain the following equations:

$$\begin{cases} \dfrac{dV_{sd}}{dt} = w_s.V_s.Cos\left(w_s.t\right) = w_s.V_{sq} \\ \dfrac{dV_{sq}}{dt} = -w_s.V_s.Sin\left(w_s.t\right) = -w_s.V_{sd} \end{cases} \quad (1)$$

With: $\begin{cases} V_{sd} = V_s.Sin\left(w_s.t\right) \\ V_{sq} = V_s.Sin\left(w_s.t + \pi/2\right) = V_s.Cos\left(w_s.t\right) \end{cases}$

It is obvious that the dynamic model Equation (31) is highly nonlinear due to the coupling between the active and reactive power. So, the study of stability of the system is characterized by:

$[X] = [P_s \quad Q_s \quad \Omega]^T$: The state vector.

$[U] = [V_{rd} \quad V_{rq}]^T$: The control variable.

The Lyapunov function is dividing in two steps, one for the control of the speed and the other for the control of the powers.

- Backstepping controller speed.

The first step of the Backstepping control defines the error of the state variable by the following calculation:

$$e_\Omega = \Omega_{ref} - \Omega \quad (37)$$

Its derivative gives:

$$\dot{e}_\Omega = \frac{de_\Omega}{dt} = \dot{\Omega}_{ref} - \dot{\Omega} \quad (38)$$

It results:

$$\dot{e}_\Omega = \dot{\Omega}_{ref} - \frac{p}{J.V_s}\phi_{sq}.P_s + \frac{p}{J.V_s}\phi_{sd}.Q_s - \frac{1}{J}T_m \quad (39)$$

Subsequently, we define the Lyapunov function by the form:

$$V_1 = \frac{1}{2}\left(e_\Omega^2\right) \quad (40)$$

Its derivative gives:

$$\begin{aligned} \dot{V}_1 = e_\Omega\dot{e}_\Omega &= e_\Omega\left(\dot{\Omega}_{ref} - \frac{p}{J.V_s}\phi_{sq}.P_s + \frac{p}{J.V_s}\phi_{sd}.Q_s - \frac{1}{J}T_m\right) \\ &= -K_\Omega.e_\Omega^2 + e_\Omega\left(K_\Omega.e_\Omega - \frac{p}{J.V_s}\phi_{sq}.P_s + \frac{p}{J.V_s}\phi_{sd}.Q_s - \frac{1}{J}T_m\right) \end{aligned} \quad (41)$$

We use the Backstepping design method to ensure the stability of the sub-system. For this, we need to make the equation (35) more negative, we consider the active and reactive powers as virtual inputs of our system and we define the following equations as:

$$\begin{cases} Q_{s\_ref} = Q_s \\ P_{s\_ref} = \dfrac{1}{\left(\dfrac{p}{J.V_s}\right).\phi_{sq}}\left(K_\Omega e_\Omega + \dfrac{p}{J.V_s}\phi_{sd}.Q_{s\_ref} - \dfrac{1}{J}T_m\right) \end{cases} \quad (42)$$

With: KΩ >0.

We substitute equation (37) in the derivative of the Lyapunov function equation V1 and we assume that Ωref is constant. As a result, we have the negativity of the function:

$$\dot{V}_1 = -K_\Omega.e_\Omega^2 \le 0 \tag{43}$$

Backstepping Controller power.

The objective of the section is to control the active and reactive powers of stator by calculating and controlling the rotor's voltages. For this, we define the following errors:

$$\begin{cases} e_{P_s} = P_{s\_ref} - P_s \\ e_{Q_s} = Q_{s\_ref} - Q_s \end{cases} \tag{44}$$

Its derivative is:

$$\begin{cases} \dot{e}_{P_s} = \dot{P}_{s\_ref} - \dot{P}_s \\ \dot{e}_{Q_s} = \dot{Q}_{s\_ref} - \dot{Q}_s \end{cases} \tag{45}$$

The control's laws of real machine are Vrd and Vrq which appear in equation (31). To analyze the stability of this system, we define a new Lyapunov function final V2 given by the following form:

$$V_2 = \frac{1}{2}\left(e_\Omega^2 + e_{P_s}^2 + e_{Q_s}^2\right) \tag{46}$$

The result of the derivative of the Lyapunov function is:

$$\begin{aligned} \dot{V}_2 \quad &= -K_\Omega.e_\Omega^2 - K_{P_s}.e_{P_s}^2 - K_{Q_s}.e_{Q_s}^2 + e_\Omega \\ &\left(K_\Omega.e_\Omega - \frac{p}{J.V_s}\phi_{sq}.P_s + \frac{p}{J.V_s}\phi_{sd}.Q_s - \frac{1}{J}T_m\right) + \\ &+e_{P_s}\left(\begin{array}{l} K_{P_s}.e_{P_s} - \left(\frac{3}{2.\sigma.L_s.L_r}\right). \\ \left(\frac{2}{3}\left(R_s.L_r + R_r.L_s\right)P_s + \right) - \omega_s.Q_s \end{array}\right) + e_{Q_s} \\ &\left(K_{Q_s}.e_{Q_s} - \left(\frac{3}{2.\sigma.L_s.L_r}\right).\left(\frac{2}{3}\left(R_s.L_r + R_r.L_s\right)Q_s + \right) + \omega_s.P_s\right) \end{aligned} \tag{47}$$

With: KΩ>0, KPs>0 and KQs>0.

The expressions of the controls voltages Vrq and Vrd are extracted from equation (43):

$$\begin{cases} V_{rd} = -\frac{1}{V_{sd}}\left(\frac{1}{M}\left(-\left(\frac{2.\sigma.L_s.L_r}{3}\right).\left(K_{P_s}.e_{P_s} - \omega_s.Q_s\right)\right)\right) \\ V_{rq} = \frac{1}{V_{sd}M}\left(\left(-\left(\frac{2.\sigma.L_s.L_r}{3}\right)(K_{Q_s}.e_{Q_s} + \omega_s.P_s)\right)\right) \end{cases} \tag{48}$$

This equation (44) implies the negativity of the Lyapunov function V2 as following:

$$V_2 \quad = -K_\Omega\, e_\Omega - K_{P_s} e_{P_s} - K_{Q_s} e_{Q_s} \le 0 \tag{49}$$

Equation (45) shows the asymptotic stability of the origin in the equations of the system of DFIG.

6.4. Application of the Backstepping Control to the Grid-Side Converter(GSC).

The main objective of the control to the grid-side converter is to stabilize the voltage and the frequency of the grid. For this we keep the DC bus voltage constant with the possibility of controlling the power factor on the grid side [16][21][32]. The grid side converter is controlled by the active and reactive powers. They are written [6]:

$$\begin{cases} P_g = V_{gd}.I_{gd} + V_{gq}.I_{gq} \\ Q_g = V_{gq}.I_{gd} - V_{gd}.I_{gq} \end{cases} \tag{50}$$

The control of the DC bus voltage makes it possible to have the reference of the grid active power. It allows us to express the expressions of the DC bus voltage as follows:

$$V_{dc}.I_{dc} = P_g - P_r \tag{51}$$

The instantaneous variations of DC Bus voltage as:

$$\frac{dV_{dc}}{dt} = \left(\frac{P_g - P_r}{C.V_{dc}}\right) \tag{52}$$

Obviously, the dynamic model is highly nonlinear due to the coupling between the power active and reactive. For this, the study of stability of the system is characterized by:

$[X] = \begin{bmatrix} P_g & Q_g & V_{dc} \end{bmatrix}^T$: The state vector.

$[U] = \begin{bmatrix} V_{gd} & V_{gq} \end{bmatrix}^T$: The control variable.

The Lyapunov function is divided in two steps, one for the control of the DC Bus voltage and the other for the control of reactive power.

- Backstepping controller DC Voltage Bus.

The first step of the Backstepping control defines the error of variable state by the following calculation:

$$e_{V_{dc}} = V_{dc\_ref} - V_{dc} \tag{53}$$

Its derivative gives:

$$\dot{e}_{V_{dc}} = \frac{de_{V_{dc}}}{dt} = \dot{V}_{dcref} - \dot{V}_{dc} \tag{54}$$

It results:

$$\begin{aligned} \dot{e}_{V_{dc}} &= \dot{V}_{dcref} - \left(\frac{P_g - P_r}{C.V_{dc}}\right) \\ &= \dot{V}_{dcref} - \left(\frac{1}{C.V_{dc}}\right).\left(\begin{array}{l} P_g - \frac{L_s}{M.V_s^2} - \frac{3}{2.M} \\ \left(\phi_{sd}.V_{rd} + \phi_{sq}.V_{rq}\right) \end{array}\right) \end{aligned} \tag{55}$$

With:

$$P_r = \frac{1}{M}.\left(\frac{L_s}{V_s^2} + \frac{3}{2}\left(\phi_{sd}.V_{rd} + \phi_{sq}.V_{rq}\right)\right)$$

Subsequently we define the Lyapunov function of the form:

$$V_1 = \frac{1}{2}\left(e_{V_{dc}}^2\right) \tag{56}$$

Its derivative gives:

$$\begin{aligned}\dot{V}_1 &= e_{V_{dc}}\dot{e}_{V_{dc}} \\ &= e_{V_{dc}}\left(\dot{V}_{dc\_ref} - \left(\frac{1}{C.V_{dc}}\right)\left(P_g - \frac{L_s}{M.V_s^2} - \frac{3}{2.M}\right)\left(\phi_{sd}.V_{rd} + \phi_{sq}.V_{rq}\right)\right) \\ &= -K_{V_{dc}}.e_{V_{dc}}^2 + e_{V_{dc}}\left(K_{V_{dc}}.e_{V_{dc}} - \left(\frac{1}{C.V_{dc}}\right)\left(P_g - \frac{L_s}{M.V_s^2} - \frac{3}{2.M}\right)\left(\phi_{sd}.V_{rd} + \phi_{sq}.V_{rq}\right)\right)\end{aligned} \tag{57}$$

We use the Backstepping design method to ensure the stability of the sub-system. For this, we need to make equation (53) more negative, we consider the active power as a virtual input of our system and we define the following equations:

$$P_{g\_ref} = \left(\frac{L_s}{M.V_s^2}\left(\left[V_{sd}.V_{rd} + V_{sq}.V_{rq}\right].P_s + \left[V_{sq}.V_{rd} + V_{sd}.V_{rq}\right].Q_s\right)\right) \tag{58}$$

With : $K_{V_{dc}} > 0$

We substitute equation (55) in the derivative of the Lyapunov function V1 equation (54), we assume that Vdcref is constant and we have the negativity of the function as:

$$\dot{V}_1 = -K_{V_{dc}}.e_{V_{dc}}^2 \le 0 \tag{59}$$

Backstepping controller Reactive power.

The objective of the section is to control the power factor of the grid side by calculating and controlling the grid voltages. For this, we define the following errors:

$$\begin{cases} e_{P_g} = P_{g\_ref} - P_g \\ e_{Q_g} = Q_{g\_ref} - Q_g \end{cases} \tag{60}$$

The results of the derivative of equation (58) are:

$$\begin{cases} \dot{e}_{P_g} = \dot{P}_{g\_ref} + \left(\frac{R_f}{L_f}\right)P_g + \omega_s.Q_g + \frac{3}{2}\left(\frac{V_{sd}}{L_f}\right)V_{gd} + \bar{V}_{gq} \\ \dot{e}_{Q_g} = \dot{Q}_{g\_ref} + \left(\frac{R_f}{L_f}\right)Q_g + \omega_s.P_g + \frac{3}{2}\left(\frac{V_{sd}}{L_f}\right)V_{gd} - \frac{3}{2}\left(\frac{V_{sq}}{L_f}\right)V_{gq} \end{cases} \tag{61}$$

The control's laws of real machine are Vgd and Vgq which appear in equation (59). Then, to analyze the stability of this system, we define a new Lyapunov function final V2 given by the following form:

$$V_2 = \frac{1}{2}\left(e_{V_{dc}}^2 + e_{P_g}^2 + e_{Q_g}^2\right) \tag{62}$$

Its derivative gives:

$$\dot{V}_2 = \begin{pmatrix} -K_{V_{dc}}.e_{V_{dc}}^2 - K_{P_g}.e_{P_g}^2 - K_{Q_g}.e_{Q_g}^2 \\ +e_{V_{dc}}\left(K_{V_{dc}}.e_{V_{dc}}\right) + e_{P_g}\begin{pmatrix} K_{P_g}.e_{P_g} + \left(\frac{R_f}{L_f}\right).P_g \\ +\omega_s.Q_g + \frac{3}{2}\left(\frac{V_{sd}}{L_f}\right). \\ V_{gd} + \bar{V}_{gq} \end{pmatrix} \end{pmatrix} \tag{63}$$

With: KVdc>0, KPg >0, and KQg>0

The expressions of the voltages grid Vgq and Vgd are extracted from equation (63) as following:

$$\begin{cases} V_{gd} = -.\left[K_{P_g}.e_{P_g} + \left(\frac{R_f}{L_f}\right)P_g + \omega_s.Q_g\right] \\ V_{gq} = .\left[K_{Q_g}.e_{Q_g} + \left(\frac{R_f}{L_f}\right)Q_g + \omega_s.P_g\right] \end{cases} \tag{64}$$

The result of the equations implies the negativity of the Lyapunov V2 function as follows:

$$V_2 = -K_{V_{dc}}e_{V_{dc}} - K_{P_g}e_{P_{gs}} - K_{Q_g}e_{Q_g} \le 0 \tag{65}$$

Equation (63) shows the asymptotic stability of the origin in the equations of the system.

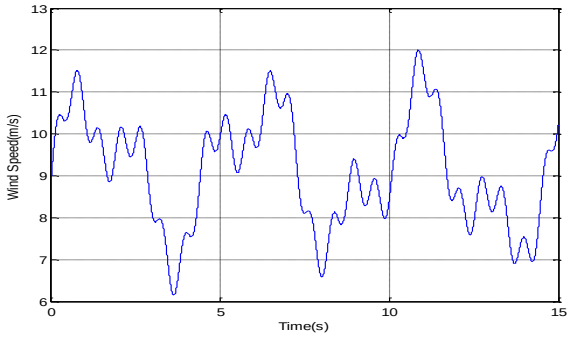

Fig. (22). Wind profile.

The fig. (**20**) shows the results obtained for this application, where the following observations can be distinguished:

- The specific speed λ and the power coefficient Cp does not change a lot of values, they are almost equal to their optimal values references 9 and 0.4999 successively;
- The wind power captured follows its optimal reference and has the same shape as the wind profile applied, this rate is also consistent with the wind torque side of the MADA;

- The speed of the DFIG is the image of wind causing the wind, it properly follows its reference;
- The shapes of the electromagnetic torque of the DFIG and its reference, are virtually identical, but different from the shape of the profile of the wind speed due to the dynamic torque due to inertia;
- The phase shift between the voltage 180 ° and the stator current phase reflects a production of active power only to the stator as illustrated in figure powers;
- The shape of the components of the stator flux orientation shows a good flow to ensure vector control well decoupled from the DFIG.

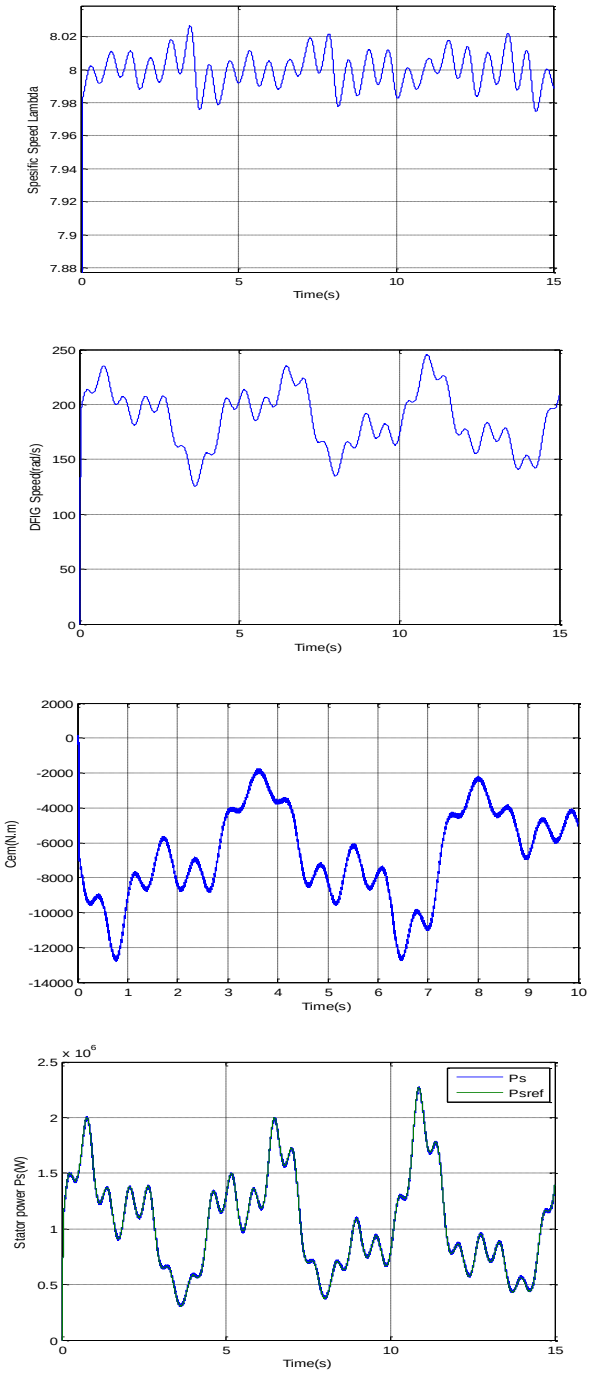

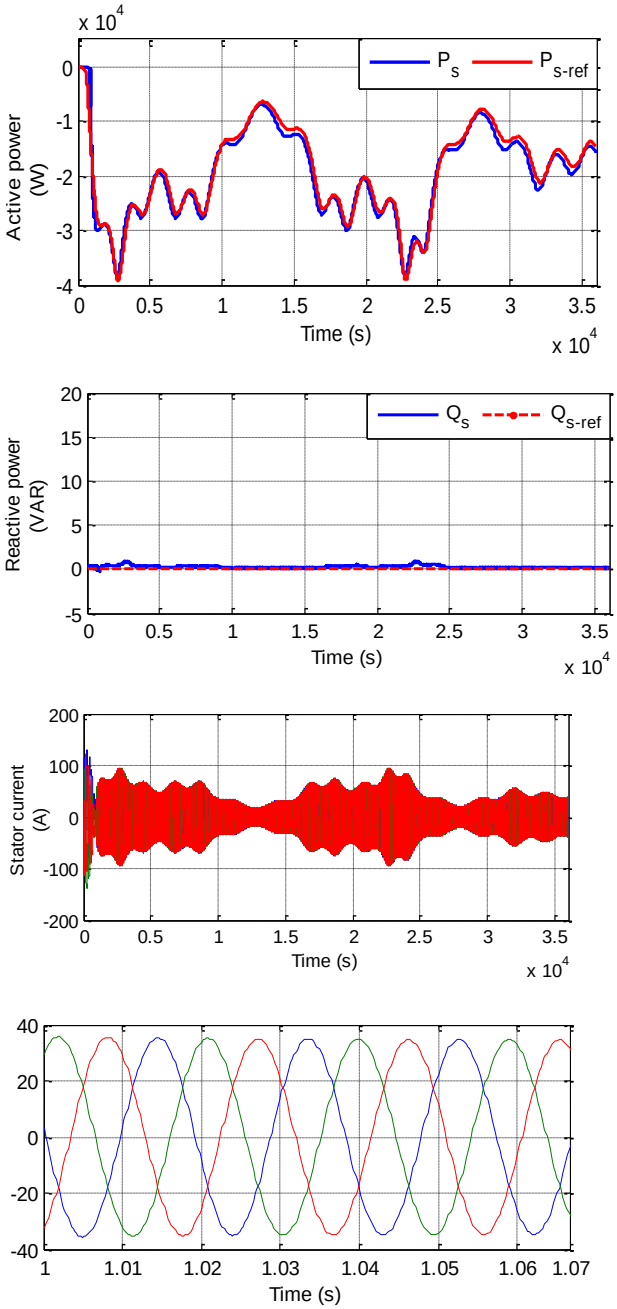

Fig. (23). The Simulation results of the asynchronous wind generator dual power and stator flux oriented, with a Backstepping controller (Case scale model of the DFIG and profile of random wind).

The figures obtained show the different performances of the wind system, which show the robustness and good tracking of the references, the specific speed and the power coefficient vary in proportion to the wind speed, which shows the reliability of the system. Active and responsive power follows their references well, making the system more robust.

7. SLIDING MODE POWER CONTROL

7.1. Sliding Mode Control Strategy

The sliding mode is a particular mode of operation of systems with variable structure. The advantage of this method is its simplicity and robustness in spite of System uncertainties and external disturbances.

The principle of this technique consists in bringing the state trajectory of a system towards the sliding surface and to switch it by means of appropriate switching logic around it to the equilibrium point, hence the phenomenon of slip.

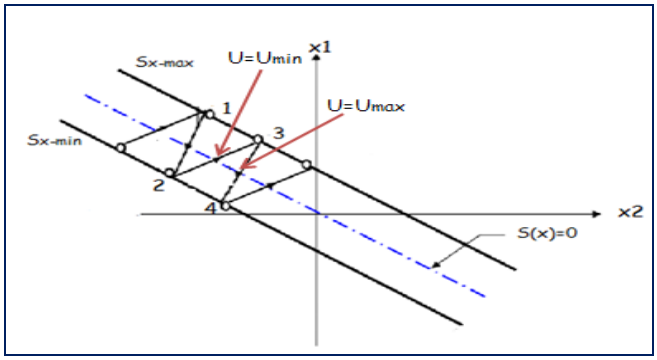

Fig. (24). The trajectory in the phase plane.

The design of the sliding mode control algorithm is carried out mainly in three complementary steps defined by [3 4].

A. sliding surfaces:

Consider the following non-linear system:

$$\dot{x} = f(x,t) + B(x,t).u(x,t) \tag{66}$$

Where :

x Є Rn: Status Vector, f(x,t) Є Rn, B(x,t) Є Rn*m , u(x,t) Є Rm : Control Vector

In order to ensure the convergence of a state variable to its reference value, it is necessary to choose a sliding surface which is a scalar function such that the variable to be adjusted slides on the latter.

J. SLOTINE proposes a form of general equation [5] [6] given by:

$$S(x) = \left(\frac{d}{dt} + \delta\right)^{n-1}.e(x) \tag{67}$$

Where :

δ: Positive gain; e(x)=xd-x : Deviation of the variable to be regulated; n: is a relative degree which represents the number of times that the surface must be derived to make the command appear .

The objective of the command is to keep the surface at zero. The latter is a linear differential equation whose unique solution is e (x) = 0.

B. Conditions of Existence and Convergence:

In order to ensure the convergence mode LYAPUNOV proposes a function V (x) which guarantees the stability of the nonlinear system and the attraction of the variable to be controlled to its reference value, the latter is defined as follows:

$$V(x) = \frac{1}{2}.S(x)^2 \succ 0 \tag{68}$$

For the function V(x) to decrease, it suffices to ensure that its derivative $V(x) = S(x).\dot{S}(x) \prec 0$. The idea is to choose a scalar function S(x)to guarantee the attraction of the variable to be controlled to its reference value, and to design a command " U " such that the square of the surface corresponds to a function of LYAPUNOV [4].

C. Determination of the control law

Once the sliding surface has been chosen, as well as the criterion of convergence, it remains to determine the control necessary to attract the state trajectory towards the surface and then towards its equilibrium point while maintaining the conditions of existence of the sliding mode.

The command (u) is a variable structure command given by [10]

$$u = \begin{cases} u^+(x) & \text{if} \quad S(x,t) \succ 0 \\ u^-(x) & \text{if} \quad S(x,t) \prec 0 \end{cases} \tag{69}$$

Where: u+ and u- are continuous functions, with u+ ≠ u-

This control (u) of discontinuous nature will force the trajectories of the system to reach the sliding surface and to remain there in the vicinity of the latter despite the presence of the disturbances.

The system trajectories on the surface S are not defined since the command (u) is not defined for S = 0, to do this, FILLIPOV [11] and UTKIN [12] propose a method called the equivalent control [10]. The addition of this command pre-positions the system in a desired stable state and in addition reduces the CHATTERING phenomenon.

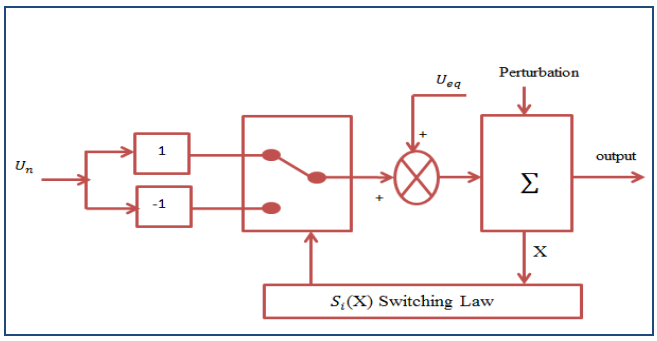

Fig. (25). The equivalent command.

This structure consists of two parts, one concerning the exact linearization (Ueq) and the other the stability (Un).

$$U = U_{eq} + U_n \tag{70}$$

(Ueq) is used to keep the variable to be controlled on the sliding surface S(x)=0. It is deduced, considering that the derivative of the surface is zero S(x)=0.

Consider the state system (17), we sought to determine the analog expression of the control U.

The derivative of the surface S (x) is given by:

$$\dot{S}(x) = \frac{\partial S}{\partial x}.f(x) + \frac{\partial S}{\partial x}.B(x).U_{eq} + \frac{\partial S}{\partial x}.B(x).U_n \tag{71}$$

In the sliding and permanent regime, the sliding surface is zero and its derivative as well as the discontinuous part is also null, so the expression of the equivalent command becomes as follows:

$$U_{eq} = -\frac{\partial S}{\partial x}.f(x).(\frac{\partial S}{\partial x}.B(x))^{-1} \tag{72}$$

It is necessary that $\frac{\partial S}{\partial x}.B(x) = 0$, so that the equivalent command can take a finite value.

By replacing the equivalent command with its expression in $\dot{S}(x)$ we obtain:

$$\dot{S}(x) = \frac{\partial S}{\partial x}.B(x).U_n \tag{73}$$

In order to satisfy the condition of attractiveness $S(x).\dot{S}(x) \prec 0$ the sign of Un must be opposed to that of $\frac{\partial S}{\partial x}.B(x).S(x)$.

The discontinuous control (Un) forces the dynamics to converge towards the surface and ensures the insensitivity of the system with respect to uncertainties and perturbations. Several forms are proposed in the literature [8] [9], the simplest one is given by:

$$U_n = K.sign(S(x)) \tag{74}$$

Where: K is a positive constant and (sign) the classical sign function.

But the main disadvantage of the relay type control is the phenomenon well known by "CHATTERING". In steady state, the latter appears as a high frequency oscillation around the equilibrium point (Fig. **6**), because of the very discontinuous nature of the sign function.

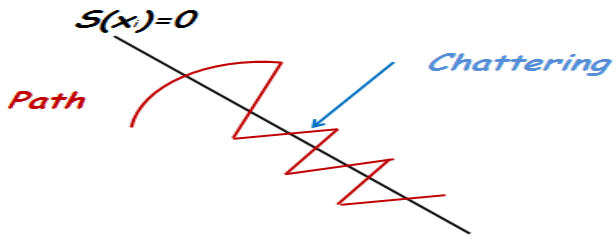

Fig. (26). Phenomenon of "CHATTERING".

To remedy this problem, several investigations have been made. One of the solutions envisaged consists in introducing a stop band around the switching surface. To do this, it suffices to replace the function (sign) with the saturation function (Sat), whose discontinuities in the vicinity of zero are less brutal. This saturation function can be expressed by [3, 4]:

$$sat(\phi) = \begin{cases} 1 & \text{if} \quad \phi \succ \varepsilon \\ +1 & \text{if} \quad \phi \prec \varepsilon \\ \frac{\phi}{\varepsilon} & \text{if} \quad |\phi| \le \varepsilon \end{cases} \tag{75}$$

D. Application of the sliding mode command to the DFIG.

After presenting the theory of sliding mode control, we will analyze in this part the application of the sliding mode control to the DFIG.

According to the flux direction control principle, the quadrature component of the stator flux is forced to zero and the direct component is equal to the total stator field.

The preceding equations become as follows:

$$\begin{cases} v_{sd} = 0 \\ v_{sq} = v_s = \omega_s.\varphi_s \\ v_{rd} = R_r.I_{rd} + \frac{d}{dt}\varphi_{rd} - \omega_r.\varphi_{rq} \\ v_{rq} = R_r.I_{rq} + \frac{d}{dt}\varphi_{rq} + \omega_r.\varphi_{rd} \end{cases} \tag{76}$$

$$\begin{cases} P_s = -V_s.\frac{M}{L_s}.I_{rq} \\ Q_s = \frac{V_s^2}{\omega_s L_s} - V_s.\frac{M}{L_s}.I_{rd} \end{cases} \tag{77}$$

$$\begin{cases} \dot{I}_{rd} = \frac{V_{rd}}{L_r.\sigma} - \frac{R_r}{L_r.\sigma}I_{rd} + \omega_r.I_{rq} \\ \dot{I}_{rq} = \frac{V_{rq}}{L_r.\sigma} - \frac{R_r}{L_r.\sigma}I_{rq} - \omega_r.I_{rd} - \omega_r.\frac{M.V_s}{L_r.L_s.\sigma.\omega_s} \end{cases} \tag{78}$$

- **Active Power Control Surface**

The sliding surface proposed by J.SLOTINE is given by:

$$S(x) = \left(\frac{d}{dt} + \delta\right)^{n-1}.e(x) \tag{79}$$

To control the active power, we take n = 1, the expression of the active power control surface is as follows:

$$S(P_s) = e(P_s) = P_{sref} - P_s \tag{80}$$

Its derivative is given by:

$$\dot{S}(P_s) = \dot{P}_{sref} - \dot{P}_s \tag{81}$$

We replace $\dot{P}_s$ by its expression as well as $\dot{I}_{rq}$ obtaining us:

$$\dot{S}(P_s) = \dot{P}_{sref} + \frac{M.V_s}{L_s}\left(\frac{V_{rq}}{L_r.\sigma} - \frac{R_r}{L_r.\sigma}I_{rq} - \omega_r.I_{rd} - \omega_r.\frac{M.V_s}{L_r.L_s.\sigma.\omega_s}\right) \tag{82}$$

By replacing the expression of Vrq with Vrqeq+ Vrqn the command clearly appears in the following equation:

$$\dot{S}(P_s) = \dot{P}_{sref} + \frac{M.V_s}{L_s}\left(\frac{V_{rqeq} + V_{rqn}}{L_r.\sigma} - \frac{R_r}{L_r.\sigma}I_{rq} - \omega_r.I_{rd} - \omega_r.\frac{M.V_s}{L_r.L_s.\sigma.\omega_s}\right) \tag{83}$$

In sliding and permanent mode: $S(P_s)=0 \Rightarrow \dot{S}(P_s)=0$ and Vrqn =0.

$$V_{rqeq} = -L_r.L_s \frac{\sigma}{M.V_s}.\dot{P}_{sref} + R_r I_{rq} + L_r \sigma.\omega_r I_{rd} + \omega_r M \frac{V_s}{L_s \omega_s} \quad (84)$$

The discontinuous control v_{rqn} is given by:

$$V_{rqn} = K_q.sat(S(P_s)) \quad (85)$$

Where: Kq is Positive gain

Reactive power control surface

We take the same surface as that of the active power:

$$S(Q_s) = e(Q_s) = Q_{sref} - Q_s \quad (86)$$

The derivative of the surface is:

$$\dot{S}(Q_s) = \dot{Q}_{sref} - \dot{Q}_s \quad (87)$$

We replace $\dot{Q}_s$ by its expression as well as $\dot{I}_{rd}$, we get:

$$\dot{S}(Q_s) = \dot{Q}_{sref} + \frac{M.V_s}{L_s}\left(\frac{V_{rd}}{L_r.\sigma} - \frac{R_r}{L_r.\sigma} I_{rd} - \omega_r.I_{rq}\right) \quad (88)$$

By replacing the expression of Vrd with Vrdeq+ Vrdn we obtain the following equation:

$$\dot{S}(Q_s) = \dot{Q}_{sref} + \frac{M.V_s}{L_s}\left(\frac{V_{rdeq} + V_{rdn}}{L_r.\sigma} - \frac{R_r}{L_r.\sigma} I_{rd} - \omega_r.I_{rq}\right) \quad (89)$$

In sliding and permanent mode: $S(Q_s)=0 \Rightarrow \dot{S}(Q_s)=0$ and Vrdn =0 .Hence, the formula of Vrdeq becomes as follow:

$$V_{rdeq} = -L_r.L_s \frac{\sigma}{M.V_s}.\dot{Q}_{sref} + R_r I_{rd} + L_r \sigma.\omega_r I_{rq} \quad (90)$$

The discontinuous control Vrdn is given by:

$$V_{rdn} = K_d.sat(S(Q_s)) \quad (91)$$

Where: Kd: Positive gain

7.2. Simulation Results

In order to validate the robustness of the sliding control applied to a DFIG-based wind system, the following figures show the results obtained from this application, where the following observations can be distinguished:

- The wind profile is given by the fig. (**7**).
- The aerodynamic power according to the MPPT has the same shape as that of the wind profile (Fig. **8**).
- The power coefficient Cp (Fig. **9**) and the specific speed (Figure 10) are kept around their optimal values 0.5505 and 8 respectively, which ensures maximum mechanical power
- The rotation speed of the machine (Fig. **11**) is less oscillating with a high reliability with respect to the input speed.
- The shape of the electromagnetic torque of the DFIG (Fig. **12**) is negative but with a shape different from that of the wind profile this is due to the dynamic torque of the inertia.
- Fig. **13** shows the active stator power and its reference profile injected into the network, where a very good decoupling can be seen between the active and reactive power of the stator.
- The stator reactive power and its reference profile are shown in Fig. **14**, which gives a unit power factor factor cos φ (φ) = 1 because (Qs) = 0) consequently a loss of iron losses.
- Fig. **15** shows the stator currents which are purely sinusoidal with a constant frequency and consequently a minimization of harmonics and therefore a better injection into the Grid.

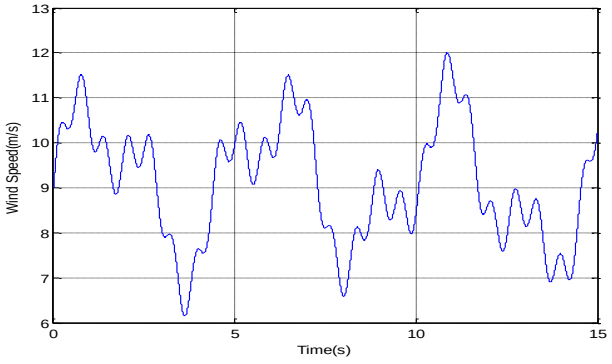

Fig. (27). Wind profile

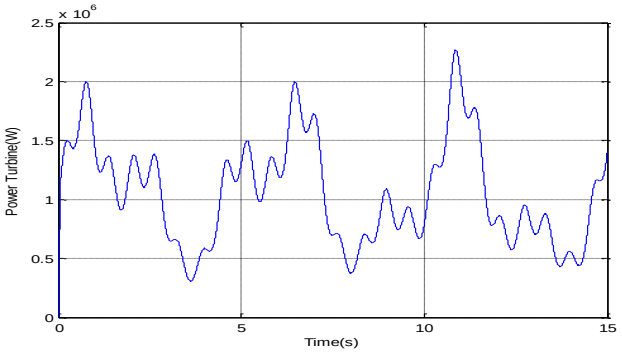

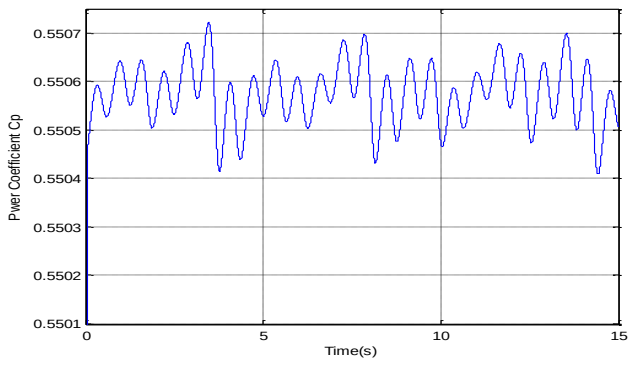

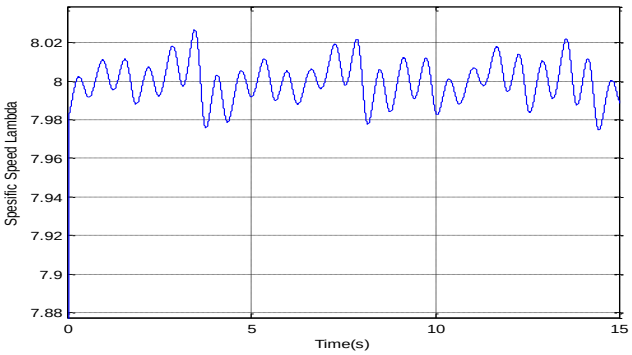

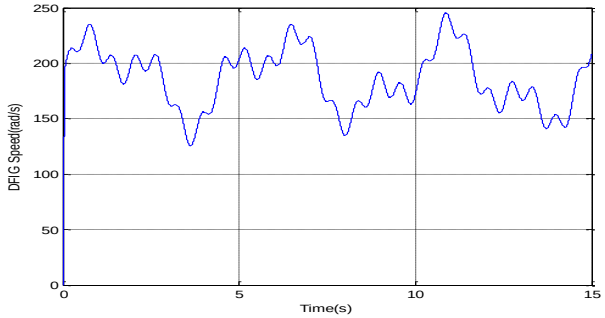

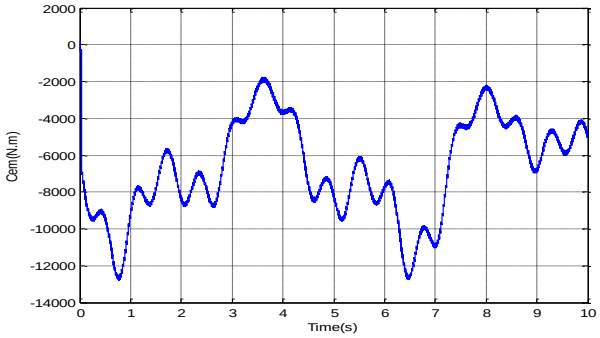

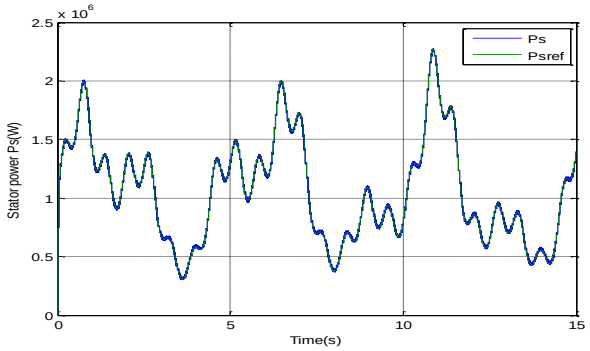

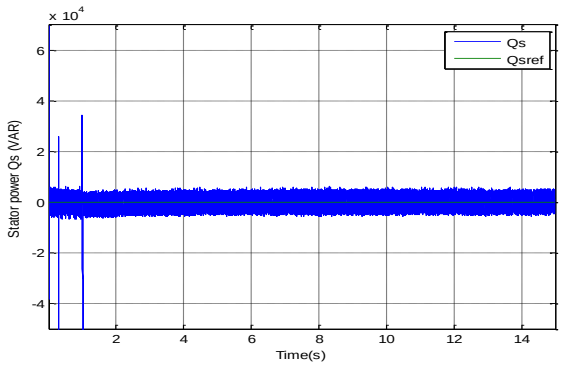

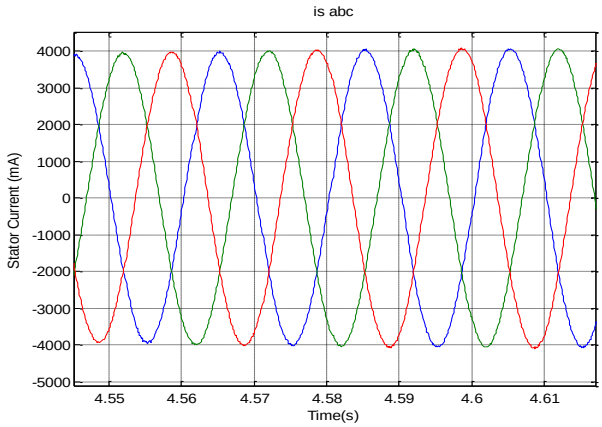

Fig. (28). The Simulation results of the asynchronous wind generator dual power, with a Sliding Mode Controller.

The figures obtained show the different performances of the wind system, which show the robustness and good tracking of the references, the specific speed and the power coefficient vary in proportion to the wind speed, which shows the reliability of the system. Active and responsive power follows their references well, making the system more robust.

8. COMPARAISON BETWEEN DIFFERENT CONTROL STRATEGY

Field Oriented Power Control
✓ Advantage: - The switching frequency is fixed; - The harmonic content of currents is well defined; - There is an application of the eight voltage vectors that can supply the voltage inverter; - Good quality of regulation of the current in steady state; ✓ Disadvantages: - The general structure of the control algorithm is complex to implement; - Transient dynamics are slower; - The parameters of the control algorithm depend on the parameters of the DFIG.
Sliding Mode Power Control
✓ Advantage: - The general structure of the control algorithm is simple to implement; - Robustness ; - The parameters of the control algorithm are independent of the parameters of the machine; - Very good dynamics during transient regimes;

✓ Disadvantages: - The zero voltage vectors are not applied.
Backstepping Power Control
✓ Advantage: - Ensures asymptotic stability and power regulation; - Correction of the speed error vector; - Very good dynamics during transient regimes; - The switching frequency is limited to half the sampling frequency; ✓ Disadvantages: - The general structure of the control algorithm is complex to implement; - Transient dynamics are slower.

9. CONCLUSION

This work was devoted to modeling, simulation and analysis of a wind turbine operating at variable speed. a use of the three linear and non-linear control techniques (Vector, Sliding Mode and Backstepping) with the application of the MPPT and Pitch Control technique, allows to improve the system performance and a better monitoring of the active and reactive power .

A comparative study between these three techniques shows that the control backstepping offers several advantages such as the robustness of the system and the linearization of the system.

CONFLICT OF INTEREST

The author declares that there are no conflicts of interest.

APPENDIX

Table 1. Parameters of the DFIG.

Rated Power	**P = 3.5 Kw**	**Stator Inductance**	**Ls = 0.084 H**
Rated Current	I = 2.0 A / 3.5 A	Rotor Inductance	Lr = 0.081 H
Rated Voltage	Vs = 220/380 V	Mutual Inductance	M = 0.078 H
Rated speed	N = 1500 rpm	Number of pole pairs	p = 2
Stator Resistance	Rs = 0.455 Ω	Moment of Inertia	J = 0.2 Kg.m^3
Rotor Resistance	Rr = 0.62 Ω		

Table 2. Parametres of Wind turbine.

Blade radius	**R= 35.25**	**Moment of Inertia**	**J = 1000 Kg.m2**
Number of blades	3	Viscous friction coefficient	f=0.0024 N.m.s-1
Gearbox ratio	G = 90	Rated wind speed	V = 15 m/s

REFERENCES

[1]. S. Pierre, C. Nichita, M.B. Camara, B. Dakyo, "Control strategy of a wind turbine simulation system designed fora hybrid wind-tidal real time emulator", 3rd Renewable Power Generation Conference (RPGTM), 24-25 September 2014, Naples, Italy.

[2]. M. Singh, S. Santoso, "Dynamic models for wind turbines and wind power plants", L/SR-5500-52780, October 2011.

[3]. B.Bossoufi, M.Karim, A.Lagrioui, M.Taoussi, A.Derouich "Observer Backstepping control of DFIG-Generators for Wind Turbines Variable-Speed: FPGA-Based Implementation" Renewable Energy Journal (ELSIVER), pp 903-917, Vol. 81. September 2015

[4]. T. Ackermann and Soder, L. « An Overview of Wind Energy-Status 2002 ». Renewable and Sustainable Energy Reviews 6(1-2), 67-127 (2002).

[5]. T. Burton, D. Sharpe, N. Jenkins and E. Bossanyi, Wind Energy Handbook. John Wiley&Sons, Ltd, 2001.

[6]. W. L. Kling and J. G. Slootweg, « Wind Turbines as Power Plants». in Proceeding of the IEEE/Cigré workshop on Wind Power and the impacts on Power Systems, 17-18 June 2002, Oslo, Norway.

[7]. D. Seyoum, C. Grantham, «Terminal Voltage Control of a Wind Turbine Driven Isolated Induction Generator using Stator Oriented Field Control». IEEE Transactions on Industry Applications, pp. 846-852, September 2003.

[8]. A. DAVIGNY, Participation aux services système de fermes éoliennes à vitesse variable intégrant un stockage inertiel d'énergie, Thèse de Doctorat, USTL Lille (France), 2007.

[9]. K. GHEDAMSI, Contribution à la modélisation et la commande d'un convertisseur direct de fréquence. Application à la conduite de la machine asynchrone, Thèse de Doctorat, ENP Alger (Algérie), 2008.

[10]. B.Bossoufi, M.Karim, S.Ionita, A.Lagrioui, "Nonlinear Non Adaptive Backstepping with Sliding-Mode Torque Control Approach for PMSM Motor" Journal of Journal of Electrical Systems JES, pp236-248. Vol.8 No.2, June 2012.

[11]. X. YU, K. STRUNZ, « Combined long-term and shortterm access storage for sustainable energy system », 2004 IEEE Power Engineering Society General Meeting, vol.2, pp.1946-1951, 10 June 2004.

[12]. S. E. Ben Elghali, « Modélisation et Commande d'une hydrolienne Equipée d'une génératrice Asynchrone Double Alimentation », JGGE'08, 16-17 Décembre 2008, Lyon (France).S

[13]. E. AIMANI, Modélisation de différentes technologies d'éoliennes intégrées dans un réseau de moyenne tension, Thèse de Doctorat, École Centrale de Lille (France), 2004.

[14]. X. YAO, C. YI, D. YING, J. GUO and L. YANG, « The grid-side PWM Converter of the Wind Power Generation System Based on Fuzzy Sliding Mode Control », Advanced Intelligent Mechatronics, IEEE 2008, Xian (Chine).

[15]. B.Bossoufi, M.Karim, S.Ionita, A.Lagrioui, "DTC control based artificial neural network for high performance PMSM drive" Journal of Theoretical and Applied Information Technology JATIT, pp165-176, Vol. 33 No.2, 30th November 2011.

[16]. B.Bossoufi, M.Karim, S.Ionita, A.Lagrioui, "Indirect Sliding Mode Control of a Permanent Magnet Synchronous Machine: FPGA-Based Implementation with Matlab & Simulink Simulation" Journal of Theoretical and Applied Information Technology JATIT, pp32-42, Vol. 29 No.1, 15th July 2011.

[17]. A. BOYETTE, « Contrôle-commande d'un générateur asynchrone à double alimentation avec système de stockage pour la production éolienne », Thèse de Doctorat, Nancy (France), 2006.

[18]. B.Bossoufi, M.Karim, S.Ionita, A.Lagrioui, "Low-Speed Sensorless Control of PMSM Motor drive Using a NONLINEAR Approach BACKSTEPPING Control: FPGA-Based Implementation" Journal of Theoretical and Applied Information Technology JATIT, pp154-166, Vol. 36 No.1, 29th February 2012.

[19]. Y.Bekakra, D.Ben Attous, "Sliding Mode Controls of Active and Reactive Power of a DFIG with MPPT for Variable Speed Wind Energy Conversion" Australian Journal of Basic and Applied Sciences, pp2274-2286, Vol 5, No.12, 2011.

[20]. L. Fan, S. Yuvarajan, R. Kavasseri," Harmonic Analysis of a DFIG for a Wind Energy Conversion System" IEEE Transactions on Energy Conversion, pp. 181-190, Vol.25, Issue 01, March 2010.

[21]. Y. Zou, M. E. Elbuluk, Y. Sozer," Stability Analysis of Maximum Power Points Tracking (MPPT) Method in Wind Power Systems" IEEE Transactions on Industry Applications, pp. 1129-1136, Vol.49, Issue 03, March 2013.

[22]. L.M. Fernandez, C.A. Garcia, F. Jurado,"Comparative study on the performance of control systems for doubly fed induction generator

(DFIG) wind turbines operating with power regulation " Journal of Elsevier of Energy, pp.1438-1452, Vol.33, Issue 09, September 2008.

[23]. B. Yang, L. Jiang, L. Wang, W. Yao, Q.H. Wu," Nonlinear maximum power point tracking control and modal analysis of DFIG based wind turbine" International Journal of Electrical Power & Energy Systems, pp. 429-436, Vol.74, January 2016.

[24]. M.Taoussi, M.Karim, B.Bossoufi, A.Lagrioui, M.El Mahfoud, "The Fuzzy Control for Rotor Flux Orientation of the doubly-fed asynchronous generator Drive", International Journal of Computers & Technology, pp 4707-4722 Vol 13 N° 08, June 15,2014.

[25]. B.Bossoufi, M.Karim, A.Lagrioui, M.Taoussi, M.L.EL Hafyani, "Backstepping Adaptive Control of DFIG-Generators for Variable-Speed Wind Turbines" I International Journal of Computers & Technology, pp3719-3733, Vol.12 No.7, February 2014.

[26]. B.Bossoufi, M.Karim, A.Lagrioui, M.Taoussi "FPGA-Based Implementation nonlinear Backstepping control of a PMSM Drive" IJPEDS International Journal of Power Electronics and Drive System, pp 12-23 Vol.4 No.1, March 2014.

[27]. M.Taoussi, M.Karim, B.Bossoufi, D. Hammoumi, A.Lagrioui," Speed Backstepping control of the doubly-fed induction machine drive", Journal of Theoretical & Applied Information Technology,pp 189-199 Vol 74 Issue 2, april 2015.

[28]. A. Junyent-Ferré, O. Gomis-Bellmunt, A. Sumper,M . Sala, M. Mata," Modeling and control of the doubly fed induction generator wind turbine" Simulation Modelling Practice and Theory , pp. 1365-1381, Vol.18, Issue 09, October 2010.

[29]. B. Bossoufi, H.A. Aroussi, E.M. Ziani, M. Karim, A. Lagrioui, A.Derouich, M. Taoussi " Robust adaptive Backstepping control approach of DFIG generators for wind turbines variable-speed" 2014 International Renewable and Sustainable Energy Conference (IRSEC), pp 791 - 797, 17-19 Oct 2014.

[30]. K. Ouari, T. Rekioua, M. Ouhrouche," Real time simulation of nonlinear generalized predictive control for wind energy conversion system with nonlinear observer" ISA Transactions, pp. 76-84, Vol.53, Issue 01, January 2014.

[31]. R. Trabelsi, A. Khedher, M. Faouzi Mimouni, F. M'sahli," Backstepping control for an induction motor using an adaptive sliding rotor-flux observer" Electric Power Systems Research, pp. 1-15, Vol.93, December 2012.

[32]. P. Xiong, D. Sun," Backstepping based DPC Strategy of Wind Turbine Driven DFIG under Normal and Harmonic Grid Voltage " IEEE Transactions on Power Electronics , pp. 4216 - 4225, Vol.31, Issue 06, June 2016.

[33]. B.Bossoufi, M.Karim, A.Lagrioui, M.Taoussi, M.L.EL Hafyani "Backstepping control of DFIG Generators for Wide-Range Variable-Speed Wind Turbines " International Journal of Automation and Control , pp 122-140, Vol.8 No.2, July 2014.

[34]. J. Hu, X. Yuan "VSC-based direct torque and reactive power control of doubly fed induction generator" Journal of Elsevier of Renewable Energy, pp. 13-23, Vol.40, Issue 01, April 2012.

[35]. G. D. Marques, M. F. Iacchetti,"Stator Frequency Regulation in a Field Oriented Controlled DFIG Connected to a DC Link" IEEE Transactions on Industrial Electronics , pp. 5930 - 5939, Vol.61, Issue 11, Nov. 2014.

[36]. B.Bossoufi, M.Karim, S.Ionita, A.Lagrioui, "The Optimal Direct Torque Control of a PMSM drive: FPGA-Based Implementation with Matlab & Simulink Simulation" Journal of Theoretical and Applied Information Technology JATIT, pp63-72, Vol. 28 No.2, 30th June 2011.

[37]. A. Gaillard, P. Poure, S. Saadate," FPGA-based reconfigurable control for switch fault tolerant operation of WECS with DFIG without redundancy" Journal of Elsevier of Renewable Energy, pp. 35-48, Vol.55, July 2013.

[38]. B.Bossoufi, M.Karim, S.Ionita, A.Lagrioui, "Low-Speed Sensorless Control of PMSM Motor drive Using a non linear Approach Backstepping Control: FPGA-Based Implementation" Journal of Theoretical and Applied Information Technology JATIT, pp154-166, Vol. 36 No.1, 29th February 2012.

[39]. D. Zhou, F. Blaabjerg, M. Lau, M. Tonnes," Optimized Reactive Power Flux of DFIG Power Converters for Better Reliability Performance Considering Grid Codes" IEEE Transactions on Industrial Electronics , pp. 1552-1562, Vol.62, Issue 03, March 2015.

[40]. J. Yao, H. Li, Z. Chen, X. Xia, X. Chen, Q. Li, Y. Liao,"Operation of Wind Turbine-Driven DFIG Systems Under Distorted Grid Voltage Conditions: Analysis and Experimental Validations" IEEE Transactions on Power Electronics , pp. 3167 - 3181, Vol.28, Issue 07, July 2013.

[41]. B.Bossoufi, M.Karim, A.Lagrioui, M.Taoussi, A.Derouich "Modeling and Backstepping Control of DFIG Generators for Wide-Range Variable-speed Wind Turbines" Journal of Journal of Electrical Systems JES, pp317-330. Vol.10 No.3, September 2014.

[42]. W. Yung-Tsai , H. Yuan-Yih ,"Reactive power control strategy for a wind farm with DFIG " Journal of Elsevier of Renewable Energy, pp. 383-390, Vol.94, August 2016.

[43]. B.Bossoufi, M.Karim, S.Ionita, A.Lagrioui, "Nonlinear Non Adaptive Backstepping with Sliding-Mode Torque Control Approach for PMSM Motor" Journal of Journal of Electrical Systems JES, pp236-248. Vol.8 No.2, June 2012.

[44]. G. Sarwar Kaloi, J. Wanga, M. Hussain Baloch," Active and reactive power control of the doubly fed induction generator based on wind energy conversion system" Journal of Elsevier of Energy Reports, pp. 194-200, Vol.02, November 2016.

[45]. M.Taoussi, M.Karim, B.Bossoufi, D.Hmmoumi, A.Lagrioui, A.Derouich "Speed Variable Adaptive Backstepping Control of the Double-Fed Induction Machine Drive" International Journal of Automation and Control (IJAAC), pp 12-33, Vol. 10, N° 01, 12 January 2016.

[46]. S. Ebrahimkhani, "Robust fractional order sliding mode control of doubly-fed induction generator (DFIG)-based wind turbines" Journal of Elsevier of ISA Transactions, pp. 343-354, Vol.63, July 2016.

[47]. D. Traoré, J. De Leon, A. Glumineau,"Adaptive interconnected observer-based Backstepping control design for sensorless induction motor" Journal of Elsevier of Automatica, pp. 682-687, Vol.48, Issue 04, April 2012.

[48]. K. Ouari, T. Rekioua, M. Ouhrouche,"Real time simulation of nonlinear generalized predictive control for wind energy conversion system with nonlinear observer" Journal of Elsevier of ISA Transactions, pp. 76-84, Vol.53, Issue 01, April 2014.

[49]. B.Bossoufi, M.Karim, S.Ionita, A.Lagrioui, "DTC control based artificial neural network for high performance PMSM Drive" Journal of Theoretical and Applied Information Technology, pp165-176, Vol. 33 No.2, 30th November 2011.

[50]. Hisn-Jang Shieh and Kuo-Kai Shyu, "Non Linear Sliding Mode Torque Control With Adaptive Backstepping Approach For Induction Motor Drive", IEEE Transactions on Industrial Electronics, pp. 380-388, Vol. 46, N° 2, April 1999.

[51]. M. Itsaso Martinez, G. Tapia, A. Susperregui, H. Camblong,"Sliding-Mode Control for DFIG Rotor-and Grid Side Converters Under Unbalanced and Harmonically Distorted Grid Voltage"IEEE Transactions on Energy Conversion , pp. 328 - 339, Vol.27, Issue 02, June 2012.